

Received April 23, 2021, accepted May 23, 2021, date of publication May 26, 2021, date of current version June 3, 2021.

Digital Object Identifier 10.1109/ACCESS.2021.3083809

Discontinuous Dynamic Analysis of a Class of 2-DOF Oscillators With Strong Nonlinearity Under a Periodic Excitation

JINJUN FAN^{ID}, MIN GAO, AND SHOULIAN CHEN

School of Mathematics and Statistics, Shandong Normal University, Jinan 250014, China

Corresponding author: Jinjun Fan (fjj18@126.com)

This work was supported in part by the Natural Science Foundation of Shandong Province under Grant ZR2019MA048, and in part by the National Natural Science Foundation of China under Grant 11971275.

ABSTRACT Starting from the car suspension system, the nonlinear characteristics of a class of two-degree-of-freedom oscillators with strong nonlinearity under a periodic excitation are discussed by the switching theory of flow in discontinuous dynamical systems. Based on the discontinuous forces and different motions of the two masses, the phase plane of each mass is composed of stick domain, nonstick domain (or free domain) and separation boundary in absolute and relative coordinates, respectively. The switching criteria between the stick and nonstick motions and the conditions of grazing motion in two different regions are developed via the G-functions and switching control laws. The mapping dynamics theory is used to give the four-dimensional transformation set and four-dimensional mapping, and the conditions for periodic motions are explored. In addition, the stick motions, two kinds of grazing motions, periodic motions for this system and a comparison of the velocities, accelerations (or forces responses) of the two masses under the two conditions of control force are simulated numerically. The results show that the stability and comfort of the vehicle can be improved by adjusting the control force, which is generated by the control unit of system or exerted by the external excitation. For further investigating the influence of system parameters on dynamical behaviors, the stick and grazing bifurcation scenarios varying with driving frequency or amplitude are also developed, which can provide useful information for parameter selection of vibration systems with clearance and the optimal design of vehicle suspension systems. This paper also has important reference value for practical applications in other industries or machinery with elastic impacts.

INDEX TERMS Discontinuous dynamical system, strong nonlinearity, switchability, stick motion, grazing motion, periodic motion.

I. INTRODUCTION

Vehicle vibration is an important factor that affects the ride comfort, stability and life of automobile parts, and serious car vibration can also affect the speed of the car and generate noise. Therefore, it is very necessary to investigate vehicle vibration and control it at the lowest level. The vibration resulted from the interaction between vehicle and road surface can be reduced by suspension system, thus an effective suspension system is essential to handling safety, reliability and other performance of vehicles. At present, the mechanism of the suspension system has been comprehensively analyzed in linear systems, but the nonlinear researches are still very

The associate editor coordinating the review of this manuscript and approving it for publication was Haibin Sun^{ID}.

poor. In fact, the nonlinear factors of vehicle suspension system have prominent influence on the stability of vehicles, see [1]–[3]. A lot of researches have been done on car suspension system, see [4]–[14]. However, many suspension systems may be affected by clearance or damping between components, which makes such systems produce strongly nonlinear, discontinuous and even more complex dynamic behaviors, so it more difficult for us to study the dynamical characteristics of this kind of oscillator. Consequently, it is a significant work to study the dynamical behaviors of such discontinuous dynamical systems.

As we all known, discontinuous dynamical systems caused by friction, impact and other factors extensively exist in mechanical engineering. For decades, numerous researches on piecewise linear dynamical systems have been carried

out. As early as in 1930, Hartog [15] considered a simple mechanical model subjected to the friction force and gave the numerical results to demonstrate the validity of periodic solution of this system. After that, an investigation on the analytic solution of a support-excited system subjected to friction was carried out via Fourier series, see [16]. Masri [17] made an experimental investigation on impact damping via a SDOF (single-degree-of-freedom) model in 1967. In 1982 and 1983, Thompson and Ghaffari [18], [19] did extensive numerical work on the resonance of impact oscillators. Moreover, a bilinear impact oscillator with an elastic constraint on the right side was discussed by using analytical methods, and a simple harmonic oscillator with a rigid constraint and a harmonic excitation was considered, which can be referred in [20], [21], respectively. With the development of science, technology and society, more and more scholars have become interested in the study of friction and impact oscillators. In 1964 and 1988, Filippov used the theory of differential inclusion and convex functions to discuss a kind of differential equation with discontinuous right-hand sides, and presented comprehensive discussion of this kind of differential equation, which can be referred in [22], [23]. In addition, further investigation of Filippov systems is available in [24]. In 2008, Bernardo *et al.* [25] described a qualitative theory for non-smooth systems and provided a method to study the bifurcation behavior of such systems. Since 1996, there have been a lot of discussions with respect to the characteristics of the non-smooth mechanical model, see [26]–[30]. The above investigations provide a lot of meaningful information and a good foundation for the analysis of discontinuous dynamics systems.

In engineering practice, the impact and friction between machine parts are very common and unavoidable, which makes the dynamical behaviors of oscillator be very complicated in discontinuous dynamical systems. In 1964, Yeh [31] gave an exact solution for steady forced vibration of a 2-DOF (two-degree-of-freedom) oscillator subjected to viscous dampers and friction. Zbiciak and Kozyra [32] investigated a dynamic problem in viscoelastic and fractional-elastic rheological models with an unilateral constraint in 2015. From 1990 to 2001, the non-smooth dynamical behaviors on beam-mass, thin-walled and elastic structures were extensively investigated by Balachandran *et al.*, see [33]–[36]. In 2004, a comprehensive approach for the design and control of mechanical systems with clearance joints was proposed, which can be applied to the prediction of the dynamical behaviors of such mechanical systems, see [37] for details. There are also numerous researches on multibody systems in bioengineering, for example, the work on the biomechanical spine in [38], and artificial hip implants in [39]. In various engineering applications, one of the most important problems of the modeling in the vibration impact system is how to select an appropriate impact model. [40] gave hard versus soft impacts in oscillatory systems modeling. Some applications of soft impact models in engineering were presented in [41]–[44], and some applications of hard impact models

can be seen [45], [46]. Moreover, [47]–[55] considered the characteristics of the discontinuous systems subjected to impulsive, Boolean control and so on.

However, there is little research on how the motion state switches at the separated boundary in the multi-degree-of-freedom oscillator. Recently, in order to study the problem of flow switching on separation boundary, Luo [56], [57] developed a systematic theory of flow switchability on separation boundary and gave the detailed introduction about this theory. This general theory was applied to study the switching criteria of flows for a discontinuous system in [58]. In the same year, Luo and Chen [59] analyzed and predicted the grazing and periodic motions of a plastic impact oscillator. In 2007, the onset and vanishing criteria of different motions in a simplified brake model were considered by Luo and Thapa, see [60]. More systematic theory on the switching control law can be seen in Luo [61]–[63]. For instance, in 2014, O'Connor and Luo [64] considered the switching criteria of motion for a friction model combined with impact. In 2018, Fan *et al.* [65] studied the passable conditions on the separation boundary of an oscillator subjected to friction force. In the same year, Sun and Fu [66] studied the discontinuous dynamical behaviors of a SDOF oscillator. Based on this general theory, many investigations on this kind of system with friction and impact have been done, and specific examples can be found in [67]–[75].

Activated by a simplified system for the active suspension system of vehicles, the aim of the work described in this paper is to investigate the dynamics of a class of 2-DOF oscillators with strong nonlinearity under a periodic excitation by the flow switching theory in discontinuous dynamical systems, which can describe the dynamic behavior of lots of mechanical components, for instance rotating members of robots and vibration dampers and so on. [1]–[13] highlighted the different technological processes used for suspension system control or focused on the method of optimal design for passive, semi-active and active vehicle suspension systems, for example sliding mode control, constrained multiobjective evolutionary search, fuzzy control and genetic algorithm etc. In above these discontinuous dynamical systems, the motion switchability, stick and grazing motions were paid little attention, therefore the discussions on the dynamical complexity of such systems were not enough. For such discontinuous dynamic system derived from the active suspension system's model of vehicles, all possible motions are considered and the formulation of switching conditions of motion is presented using recent switching theory of flow, and at the same time the numerical simulation for several typical motions and stick and grazing bifurcation scenarios varying with driving frequency or amplitude are further given.

In this paper, the physical model of an active suspension system of vehicles will be introduced first. Owing to the clearance existing in the system, the phase plane of this system is partitioned into stick domains, nonstick domains (or free domains) by separation boundaries in absolute and relative frames, respectively. Furthermore, the switching criteria

between the stick and nonstick motions and the conditions of grazing motion in two different regions can be presented based on the G-functions at discontinuous boundaries. By employing the mapping dynamics theory, the four-dimensional transformation set and four-dimensional mapping are given and the conditions for periodic motions are developed. Combined with the criteria of occurrence for all kinds of motions, the stick motions, two kinds of grazing motions and periodic motions for this system are simulated numerically. Finally, the comparison of the velocities and accelerations (or forces responses) for the two masses under the two conditions of control force, and the stick and grazing bifurcation scenarios varying with driving frequency or amplitude are further carried out to better demonstrate the dynamical behaviors in such system.

II. DESCRIPTION OF PROBLEM

Based on the car suspension system, a 2-DOF mechanical model with strong nonlinearity under a periodic excitation is considered in this paper, and the two masses $m^{(1)}$, $m^{(2)}$ and a base in physical model stand for the wheel, car body and the ground, respectively. As sketched in Fig. 1, there are three components connected by two vertical linear springs of suspension stiffness coefficients k_i and two dampers of suspension damping coefficients c_i ($i = 1, 2$); and a combined device consisting of a spring of stiffness coefficient k_3 and a damper of damping coefficients c_3 is fixed on the mass $m^{(1)}$. The distance between the mass $m^{(2)}$ and the combined device is e when they are in their respective equilibrium positions. X is the road profile function acting on the base, which is set as a simple harmonic function in this paper, i.e., $X(t) = A \sin \Omega t$, where A and Ω are the excitation amplitude and frequency, respectively. As a consequence, if the road profile is assumed to be harmonic, the horizontal speed v of the car is constant and the wavelength is l , then we have the frequency $\Omega = \frac{2\pi v}{l}$. This car suspension model is limited to discuss the dynamical behavior in the vertical direction only. The origins of coordinates for the two masses $m^{(1)}$, $m^{(2)}$ and the base are set as their respective equilibrium positions. $x^{(\alpha)}$ and X denote the vertical displacement of the masses $m^{(\alpha)}$ ($\alpha = 1, 2$) and the base, respectively. In this model, the control force (i.e., desired actuator force) $f(t)$ between body mass and wheel mass, which depends on acceleration and velocity of car body and the deflection speed of car body relative to wheel, can be created by a unit (for example, a fuzzy logic controller in [12]). The vehicle is assumed to move with a constant forward speed v to model the road input, then the vertical velocity can be taken as a white noise process which is approximately true for most of real roadways. The base is affected by a road profile function $X(t)$, thus the equation of motion of the base reads

$$X(t) = A \sin \Omega t, \dot{X}(t) = A\Omega \cos \Omega t, \ddot{X}(t) = -A\Omega^2 \sin \Omega t, \quad (1)$$

where $\dot{X} = dX/dt$.

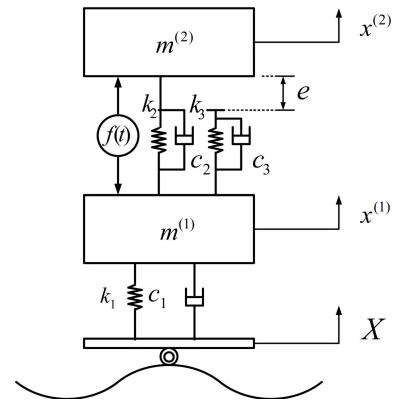


FIGURE 1. Physical model.

For this system, due to the limited clearance between the masses $m^{(\alpha)}$ ($\alpha = 1, 2$), the motion states of each mass can be divided into two categories: nonstick motion (or free motion) and stick motion. If the mass $m^{(2)}$ does not reach to the combined device, or the third linear spring is not compressed (i.e., $x^{(1)} - x^{(2)} \leq e$), this motion is called nonstick motion (or free motion). If the mass $m^{(2)}$ reaches to the combined device and the third linear spring is compressed (i.e., $x^{(1)} - x^{(2)} > e$), then the two masses move together under the effect of the third linear spring and damper, this motion is called stick motion.

When the mass $m^{(2)}$ moves freely, its behavior is only affected by the second linear spring and damper and the control force. In other words, when both the two masses are moving freely, they are not affected by the force of the third linear spring and damper. According to the above analysis, the equations for the masses $m^{(1)}$ and $m^{(2)}$ during the nonstick motion can be given by using Newton's second law, i.e.,

$$\begin{cases} m^{(1)}\ddot{x}^{(1)} + k_2(x^{(1)} - x^{(2)}) + c_2(\dot{x}^{(1)} - \dot{x}^{(2)}) = -k_1(x^{(1)} - X) - c_1(\dot{x}^{(1)} - \dot{X}) - f(t), \\ m^{(2)}\ddot{x}^{(2)} + k_2(x^{(2)} - x^{(1)}) + c_2(\dot{x}^{(2)} - \dot{x}^{(1)}) = f(t), \end{cases} \quad (2)$$

where $\ddot{x}^{(\alpha)}$ and $\dot{x}^{(\alpha)}$ stand for the acceleration and velocity of the mass $m^{(\alpha)}$ ($\alpha \in \{1, 2\}$), respectively.

When the mass $m^{(2)}$ reaches to the combined device and moves together with it, the behaviors of two masses $m^{(\alpha)}$ ($\alpha = 1, 2$) are affected by the third linear spring and damper. Therefore, the equations for the masses $m^{(\alpha)}$ ($\alpha = 1, 2$) during the stick motion are written as

$$\begin{cases} m^{(1)}\ddot{x}^{(1)} + k_2(x^{(1)} - x^{(2)}) + c_2(\dot{x}^{(1)} - \dot{x}^{(2)}) + k_3(x^{(1)} - x^{(2)} - e) + c_3(\dot{x}^{(1)} - \dot{x}^{(2)}) = -k_1(x^{(1)} - X) - c_1(\dot{x}^{(1)} - \dot{X}) - f(t), \\ m^{(2)}\ddot{x}^{(2)} + k_2(x^{(2)} - x^{(1)}) + c_2(\dot{x}^{(2)} - \dot{x}^{(1)}) - k_3(x^{(1)} - x^{(2)} - e) - c_3(\dot{x}^{(1)} - \dot{x}^{(2)}) = f(t). \end{cases} \quad (3)$$

For simplicity of notation, we give the following symbols

$$\begin{aligned} A^{(\alpha)} &= \frac{k_2}{m^{(\alpha)}}, & B^{(\alpha)} &= \frac{c_2}{m^{(\alpha)}}, & C^{(\alpha)} &= \frac{k_3}{m^{(\alpha)}}, & D^{(\alpha)} &= \frac{c_3}{m^{(\alpha)}}, \\ E^{(\alpha)} &= \frac{f(t)}{m^{(\alpha)}}, & \eta^{(1)} &= \frac{k_1}{m^{(1)}}, & \xi^{(1)} &= \frac{c_1}{m^{(1)}}, \end{aligned} \quad (4)$$

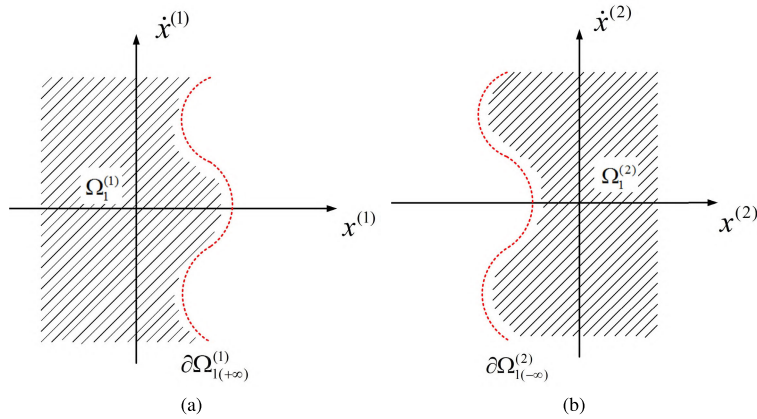


FIGURE 2. Absolute domains and boundaries without stick: (a) mass $m^{(1)}$ and (b) mass $m^{(2)}$.

where $\alpha = 1, 2$. Therefore, the equations of nonstick motion for this mechanical model are

$$\begin{cases} \ddot{x}^{(1)} + A^{(1)}(x^{(1)} - x^{(2)}) + B^{(1)}(\dot{x}^{(1)} - \dot{x}^{(2)}) = -\eta^{(1)}(x^{(1)} - X) \\ \quad -\xi^{(1)}(\dot{x}^{(1)} - \dot{X}) - E^{(1)}, \\ \ddot{x}^{(2)} + A^{(2)}(x^{(2)} - x^{(1)}) + B^{(2)}(\dot{x}^{(2)} - \dot{x}^{(1)}) = E^{(2)}, \end{cases} \quad (5)$$

and the equations of stick motion for this mechanical model are

$$\begin{cases} \ddot{x}^{(1)} + A^{(1)}(x^{(1)} - x^{(2)}) + B^{(1)}(\dot{x}^{(1)} - \dot{x}^{(2)}) + C^{(1)}(x^{(1)} - x^{(2)} - e) \\ \quad + D^{(1)}(\dot{x}^{(1)} - \dot{x}^{(2)}) = -\eta^{(1)}(x^{(1)} - X) - \xi^{(1)}(\dot{x}^{(1)} - \dot{X}), \\ -E^{(1)}\dot{x}^{(2)} + A^{(2)}(x^{(2)} - x^{(1)}) + B^{(2)}(\dot{x}^{(2)} - \dot{x}^{(1)}) \\ \quad - C^{(1)}(x^{(1)} - x^{(2)} - e) - D^{(1)}(\dot{x}^{(1)} - \dot{x}^{(2)}) = E^{(2)}. \end{cases} \quad (6)$$

III. DOMAINS AND BOUNDARIES

Based on the above discussion, the force acting on the mass $m^{(\alpha)}$ ($\alpha \in \{1, 2\}$) is discontinuous, and the phase plane is composed of two different domains including nonstick domain and stick domain and a discontinuous boundary for each mass. In order to better study the motions in different domains and transformation mechanism of motion at discontinuous boundaries for each mass, the division of the phase space in absolute and relative frames will be given in the following two subsections, respectively. Hereinafter, the origins of coordinates for each mass and the base are set as their respective equilibrium positions.

A. DOMAINS AND BOUNDARIES IN ABSOLUTE COORDINATES

Consider the nonstick motions for the masses $m^{(\alpha)}$ ($\alpha = 1, 2$) first. The corresponding named regions $\Omega_1^{(\alpha)}$ ($\alpha = 1, 2$) are

$$\begin{cases} \Omega_1^{(1)} = \{x^{(1)}, \dot{x}^{(1)} | x^{(1)} \in (-\infty, x^{(2)} + e), \dot{x}^{(1)} \in (-\infty, +\infty)\}, \\ \Omega_1^{(2)} = \{x^{(2)}, \dot{x}^{(2)} | x^{(2)} \in (x^{(1)} - e, +\infty), \dot{x}^{(2)} \in (-\infty, +\infty)\}, \end{cases} \quad (7)$$

and the separation boundaries $\partial\Omega_{1(+\infty)}^{(1)}$ and $\partial\Omega_{1(-\infty)}^{(2)}$ are introduced as

$$\begin{cases} \partial\Omega_{1(+\infty)}^{(1)} = \{x^{(1)}, \dot{x}^{(1)} | \varphi_{1(+\infty)}^{(1)} \equiv x^{(1)} - x^{(2)} - e = 0, \\ \quad \dot{x}^{(1)} \in (-\infty, +\infty)\}, \\ \partial\Omega_{1(-\infty)}^{(2)} = \{x^{(2)}, \dot{x}^{(2)} | \varphi_{1(-\infty)}^{(2)} \equiv x^{(2)} - x^{(1)} + e = 0, \\ \quad \dot{x}^{(2)} \in (-\infty, +\infty)\}, \end{cases} \quad (8)$$

where the subscripts $\pm\infty$ stand for the permanent boundaries, herein assume that the mass $m^{(2)}$ cannot reach the combined device. The above absolute domains $\Omega_1^{(\alpha)}$ ($\alpha = 1, 2$) and the separation boundaries $\partial\Omega_{1(+\infty)}^{(1)}$ and $\partial\Omega_{1(-\infty)}^{(2)}$ are sketched in Fig. 2. With the assumption that the mass $m^{(2)}$ cannot move together with the combined device, the separation boundaries are permanent impassable boundaries. The shaded regions denote the nonstick (or free) motion domains $\Omega_1^{(\alpha)}$ ($\alpha = 1, 2$) for the masses $m^{(\alpha)}$ ($\alpha = 1, 2$), and the red dashed curves stand for the separation boundaries $\partial\Omega_{1(+\infty)}^{(1)}$ and $\partial\Omega_{1(-\infty)}^{(2)}$.

For this 2-DOF mechanical model, the stick motion for the mass $m^{(2)}$ touching with the combined device can occur under appropriate conditions. For this case, the phase plane can be divided into new domains by boundaries. The absolute stick domains $\Omega_0^{(\alpha)}$ and the nonstick domains $\Omega_1^{(\alpha)}$ ($\alpha = 1, 2$) for the masses $m^{(\alpha)}$ ($\alpha = 1, 2$) are expressed by

$$\begin{cases} \Omega_0^{(1)} = \{x^{(1)}, \dot{x}^{(1)} | x^{(1)} \in (x_{cr}^{(2)} + e, +\infty), \dot{x}^{(1)} \in (-\infty, +\infty)\}, \\ \Omega_0^{(2)} = \{x^{(2)}, \dot{x}^{(2)} | x^{(2)} \in (-\infty, x_{cr}^{(1)} - e), \dot{x}^{(2)} \in (-\infty, +\infty)\}, \\ \Omega_1^{(1)} = \{x^{(1)}, \dot{x}^{(1)} | x^{(1)} \in (-\infty, x_{cr}^{(2)} + e), \dot{x}^{(1)} \in (-\infty, +\infty)\}, \\ \Omega_1^{(2)} = \{x^{(2)}, \dot{x}^{(2)} | x^{(2)} \in (x_{cr}^{(1)} - e, +\infty), \dot{x}^{(2)} \in (-\infty, +\infty)\}, \end{cases} \quad (9)$$

where $x_{cr}^{(\alpha)}$ are the critical displacements of the masses $m^{(\alpha)}$ ($\alpha = 1, 2$) for appearance or vanishing of the stick motion with $x_{cr}^{(1)} - x_{cr}^{(2)} = e$. The corresponding absolute displacement boundaries are defined as

$$\begin{cases} \partial\Omega_{01}^{(1)} = \{x^{(1)}, \dot{x}^{(1)} | \varphi_{01}^{(1)} \equiv x^{(1)} - x_{cr}^{(2)} - e = 0, \dot{x}^{(1)} < \dot{x}_{cr}^{(2)}\}, \\ \partial\Omega_{01}^{(2)} = \{x^{(2)}, \dot{x}^{(2)} | \varphi_{01}^{(2)} \equiv x^{(2)} - x_{cr}^{(1)} + e = 0, \dot{x}^{(2)} > \dot{x}_{cr}^{(1)}\}, \\ \partial\Omega_{10}^{(1)} = \{x^{(1)}, \dot{x}^{(1)} | \varphi_{10}^{(1)} \equiv x^{(1)} - x_{cr}^{(2)} - e = 0, \dot{x}^{(1)} > \dot{x}_{cr}^{(2)}\}, \\ \partial\Omega_{10}^{(2)} = \{x^{(2)}, \dot{x}^{(2)} | \varphi_{10}^{(2)} \equiv x^{(2)} - x_{cr}^{(1)} + e = 0, \dot{x}^{(2)} < \dot{x}_{cr}^{(1)}\}, \end{cases} \quad (10)$$

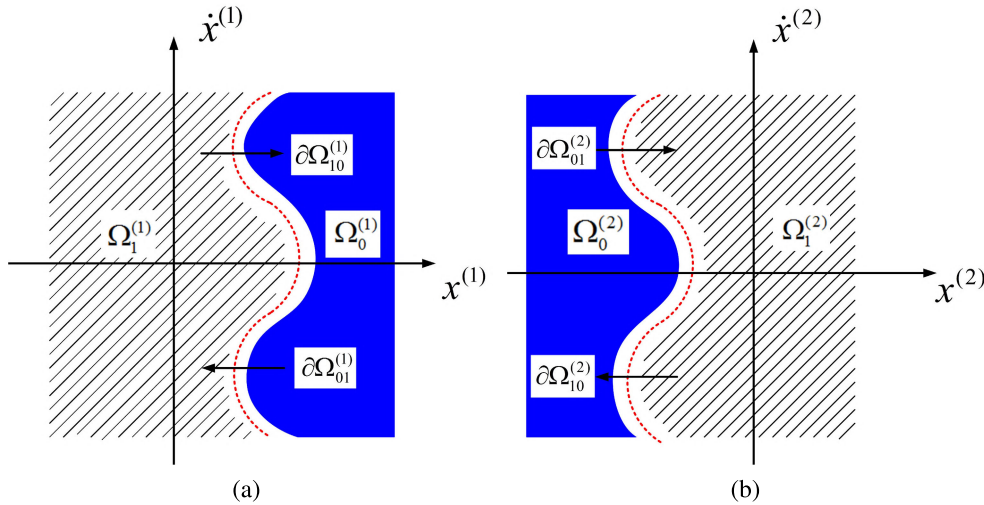


FIGURE 3. Absolute domains and boundaries with stick: (a) mass $m^{(1)}$ and (b) mass $m^{(2)}$.

where the $\dot{x}_{cr}^{(\alpha)}$ denote the critical velocity of the masses $m^{(\alpha)}$ ($\alpha = 1, 2$) for the appearance and vanishing of the stick motion. The above domains $\Omega_0^{(\alpha)}$, $\Omega_1^{(\alpha)}$ and boundaries $\partial\Omega_{10}^{(\alpha)}$, $\partial\Omega_{01}^{(\alpha)}$ ($\alpha = 1, 2$) are plotted in Fig. 3. The blue domain $\Omega_0^{(\alpha)}$ and shaded region $\Omega_1^{(\alpha)}$ ($\alpha \in \{1, 2\}$) stand for the domains of stick motion and nonstick motion for the mass $m^{(\alpha)}$ ($\alpha \in \{1, 2\}$), respectively. The boundaries $\partial\Omega_{10}^{(\alpha)}$, $\partial\Omega_{01}^{(\alpha)}$ ($\alpha \in \{1, 2\}$) represented by the red dashed curves denote the displacement boundaries when the stick motion of the object appears or disappears, and the black arrows indicate the direction in which the domain flows pass through the corresponding boundary in Fig. 3. For this 2-DOF oscillator with strong nonlinearity under a periodic excitation, herein we define the vectors of the flow and the corresponding vector field as

$$\mathbf{x}_\lambda^{(\alpha)} \triangleq (x_\lambda^{(\alpha)}, \dot{x}_\lambda^{(\alpha)}), \mathbf{F}_\lambda^{(\alpha)} \triangleq (\dot{x}_\lambda^{(\alpha)}, F_\lambda^{(\alpha)})^T, \lambda=0, 1 \text{ and } \alpha=1, 2, \quad (11)$$

where the superscript α stands for the mass $m^{(\alpha)}$ ($\alpha \in \{1, 2\}$), and $\lambda = 0$ and $\lambda = 1$ represent the stick motion in domain $\Omega_0^{(\alpha)}$ and nonstick motion in domain $\Omega_1^{(\alpha)}$ ($\alpha \in \{1, 2\}$), respectively. Then the equations of motion in absolute frame for the mass $m^{(\alpha)}$ can be rewritten as

$$\dot{\mathbf{x}}_\lambda^{(\alpha)} = \mathbf{F}_\lambda^{(\alpha)}(\mathbf{x}_\lambda^{(\alpha)}, \mathbf{x}_\lambda^{(\bar{\alpha})}, t), \quad \lambda = 0, 1, \quad (12)$$

where $\alpha \neq \bar{\alpha} \in \{1, 2\}$; and

$$\begin{cases} F_1^{(1)}(\mathbf{x}_\lambda^{(1)}, \mathbf{x}_\lambda^{(2)}, t) = -A^{(1)}(x_\lambda^{(1)} - x_\lambda^{(2)}) - B^{(1)}(\dot{x}_\lambda^{(1)} - \dot{x}_\lambda^{(2)}) \\ \quad - \eta^{(1)}(x_\lambda^{(1)} - X) - \xi^{(1)}(\dot{x}_\lambda^{(1)} - \dot{X}) - E^{(1)}, \\ F_1^{(2)}(\mathbf{x}_\lambda^{(2)}, \mathbf{x}_\lambda^{(1)}, t) = -A^{(2)}(x_\lambda^{(2)} - x_\lambda^{(1)}) \\ \quad - B^{(2)}(\dot{x}_\lambda^{(2)} - \dot{x}_\lambda^{(1)}) + E^{(2)} \end{cases} \quad (13)$$

for the nonstick motion ($\lambda = 1$); and

$$\begin{cases} F_0^{(1)}(\mathbf{x}_\lambda^{(1)}, \mathbf{x}_\lambda^{(2)}, t) \\ = -A^{(1)}(x_\lambda^{(1)} - x_\lambda^{(2)}) - B^{(1)}(\dot{x}_\lambda^{(1)} - \dot{x}_\lambda^{(2)}) \\ \quad - C^{(1)}(x_\lambda^{(1)} - x_\lambda^{(2)} - e) - D^{(1)}(\dot{x}_\lambda^{(1)} - \dot{x}_\lambda^{(2)}) \\ \quad - \eta^{(1)}(x_\lambda^{(1)} - X) - \xi^{(1)}(\dot{x}_\lambda^{(1)} - \dot{X}) - E^{(1)}, \\ F_0^{(2)}(\mathbf{x}_\lambda^{(2)}, \mathbf{x}_\lambda^{(1)}, t) \\ = -A^{(2)}(x_\lambda^{(2)} - x_\lambda^{(1)}) - B^{(2)}(\dot{x}_\lambda^{(2)} - \dot{x}_\lambda^{(1)}) \\ \quad + C^{(1)}(x_\lambda^{(1)} - x_\lambda^{(2)} - e) + D^{(1)}(\dot{x}_\lambda^{(1)} - \dot{x}_\lambda^{(2)}) + E^{(2)} \end{cases} \quad (14)$$

for the stick motion ($\lambda = 0$).

B. DOMAINS AND BOUNDARIES IN RELATIVE COORDINATES

In absolute coordinates, all the boundaries in phase plane are varying with time, and the appearance and vanishing of stick motion are dependent on the relative displacement and relative velocity in such suspension system of vehicles. Hence, it is very difficult to obtain the criteria for stick, nonstick and grazing motions of each object for such system in absolute coordinates. Therefore, it is necessary to introduce relative coordinates for the masses $m^{(1)}$ and $m^{(2)}$ herein. The relative displacement, velocity and acceleration of the mass $m^{(\alpha)}$ ($\alpha \in \{1, 2\}$) to the mass $m^{(\bar{\alpha})}$ are defined as

$$z^{(\alpha)} = x^{(\alpha)} - x^{(\bar{\alpha})}, \dot{z}^{(\alpha)} = \dot{x}^{(\alpha)} - \dot{x}^{(\bar{\alpha})}, \ddot{z}^{(\alpha)} = \ddot{x}^{(\alpha)} - \ddot{x}^{(\bar{\alpha})}, \quad (15)$$

where $i \neq \bar{i} \in \{1, 2\}$. The relative domains and boundaries for the mass $m^{(\alpha)}$ ($\alpha \in \{1, 2\}$) are sketched in Fig. 4. The stick domain $\Omega_0^{(\alpha)}$ and nonstick domain $\Omega_1^{(\alpha)}$ ($\alpha \in \{1, 2\}$) are plotted by blue areas and shaded regions, respectively. The displacement boundary $\partial\Omega_{01}^{(\alpha)}$ or $\partial\Omega_{10}^{(\alpha)}$ ($\alpha \in \{1, 2\}$) is independent of time and becomes a straight line represented by red dashed curves as plotted in Fig. 4.

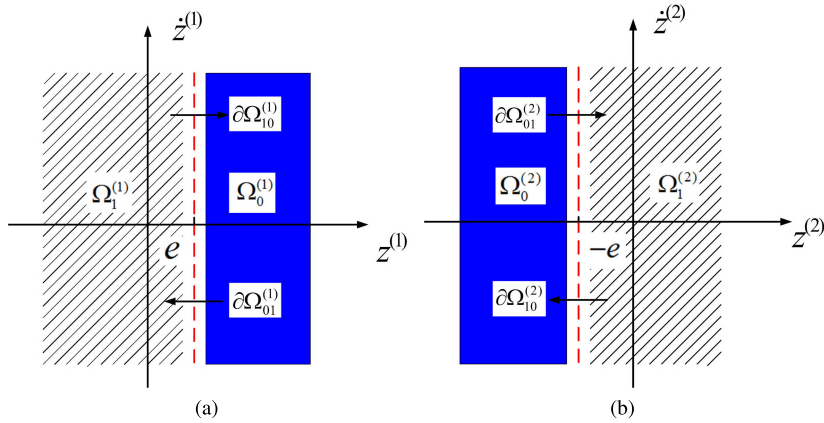


FIGURE 4. Relative domains and boundaries with stick: (a) mass $m^{(1)}$ and (b) mass $m^{(2)}$.

The relative stick domain $\Omega_0^{(\alpha)}$ and nonstick domain $\Omega_1^{(\alpha)}$ for motion of the mass $m^{(\alpha)}$ ($\alpha \in \{1, 2\}$) are defined by

$$\begin{cases} \Omega_0^{(1)} = \{(z^{(1)}, \dot{z}^{(1)}) | z^{(1)} \in (e, +\infty), \dot{z}^{(1)} \in (-\infty, +\infty)\}, \\ \Omega_0^{(2)} = \{(z^{(2)}, \dot{z}^{(2)}) | z^{(2)} \in (-\infty, -e), \dot{z}^{(2)} \in (-\infty, +\infty)\}, \\ \Omega_1^{(1)} = \{(z^{(1)}, \dot{z}^{(1)}) | z^{(1)} \in (-\infty, e), \dot{z}^{(1)} \in (-\infty, +\infty)\}, \\ \Omega_1^{(2)} = \{(z^{(2)}, \dot{z}^{(2)}) | z^{(2)} \in (-e, +\infty), \dot{z}^{(2)} \in (-\infty, +\infty)\}, \end{cases} \quad (16)$$

and the relative displacement boundary $\partial\Omega_{01}^{(\alpha)}$ or $\partial\Omega_{10}^{(\alpha)}$ of the mass $m^{(\alpha)}$ ($\alpha \in \{1, 2\}$) is given by

$$\begin{cases} \partial\Omega_{01}^{(1)} = \{(z^{(1)}, \dot{z}^{(1)}) | \varphi_{01}^{(1)} \equiv z_{cr}^{(1)} - e = 0, \dot{z}^{(1)} < 0\}, \\ \partial\Omega_{01}^{(2)} = \{(z^{(2)}, \dot{z}^{(2)}) | \varphi_{01}^{(2)} \equiv z_{cr}^{(2)} + e = 0, \dot{z}^{(2)} > 0\}, \\ \partial\Omega_{10}^{(1)} = \{(z^{(1)}, \dot{z}^{(1)}) | \varphi_{10}^{(1)} \equiv z_{cr}^{(1)} - e = 0, \dot{z}^{(1)} > 0\}, \\ \partial\Omega_{10}^{(2)} = \{(z^{(2)}, \dot{z}^{(2)}) | \varphi_{10}^{(2)} \equiv z_{cr}^{(2)} + e = 0, \dot{z}^{(2)} < 0\}, \end{cases} \quad (17)$$

where the boundary $\partial\Omega_{01}^{(\alpha)}$ or $\partial\Omega_{10}^{(\alpha)}$ is the displacement (or stick) boundary of the mass $m^{(\alpha)}$ ($\alpha \in \{1, 2\}$), and $z_{cr}^{(\alpha)}$ stands for the relative displacement of the mass $m^{(\alpha)}$ ($\alpha \in \{1, 2\}$) for the appearance or vanishing of the stick motion.

In relative frames, the state vector and vector of vector field for the mass $m^{(\alpha)}$ ($\alpha \in \{1, 2\}$) are defined as

$$\mathbf{z}_\lambda^{(\alpha)} \triangleq (z_\lambda^{(\alpha)}, \dot{z}_\lambda^{(\alpha)}), \quad \mathbf{g}_\lambda^{(\alpha)} \triangleq (\dot{z}_\lambda^{(\alpha)}, g_\lambda^{(\alpha)})^T, \quad \lambda = 0, 1, \quad (18)$$

where $\lambda = 0$ and $\lambda = 1$ represent the stick motion in domain $\Omega_0^{(\alpha)}$ and nonstick motion in domain $\Omega_1^{(\alpha)}$, respectively. Then the equation of motion of the vector form for the mass $m^{(\alpha)}$ ($\alpha \in \{1, 2\}$) in relative frames is

$$\dot{\mathbf{z}}_\lambda^{(\alpha)} = \mathbf{g}_\lambda^{(\alpha)}(\mathbf{z}_\lambda^{(\alpha)}, \mathbf{x}_\lambda^{(\bar{\alpha})}, t) \quad \text{with} \quad \dot{\mathbf{x}}_\lambda^{(\bar{\alpha})} = \mathbf{F}_\lambda^{(\bar{\alpha})}(\mathbf{x}_\lambda^{(\bar{\alpha})}, \mathbf{x}_\lambda^{(\alpha)}, t), \quad (19)$$

where $\lambda = 0, 1$, $\alpha \neq \bar{\alpha} \in \{1, 2\}$; and

$$\begin{cases} g_1^{(1)} = -(A^{(1)} + A^{(2)})z_1^{(1)} - (B^{(1)} + B^{(2)})\dot{z}_1^{(1)} \\ \quad - \eta^{(1)}(z_1^{(1)} + x_1^{(2)} - X) - \xi^{(1)}(\dot{z}_1^{(1)} + \dot{x}_1^{(2)} - \dot{X}) \\ \quad - E^{(1)} - E^{(2)}, \\ g_1^{(2)} = (A^{(1)} + A^{(2)})z_1^{(1)} + (B^{(1)} + B^{(2)})\dot{z}_1^{(1)} \\ \quad + \eta^{(1)}(x_1^{(1)} - X) + \xi^{(1)}(\dot{x}_1^{(1)} - \dot{X}) \\ \quad + E^{(1)} + E^{(2)} \end{cases} \quad (20)$$

for the nonstick motion ($\lambda = 1$); and

$$\begin{cases} g_0^{(1)} = -(A^{(1)} + A^{(2)})z_0^{(1)} - (B^{(1)} + B^{(2)})\dot{z}_0^{(1)} \\ \quad - \eta^{(1)}(z_0^{(1)} + x_0^{(2)} - X) - \xi^{(1)}(\dot{z}_0^{(1)} + \dot{x}_0^{(2)} - \dot{X}) \\ \quad - 2C^{(1)}(z_0^{(1)} - e) - 2D^{(1)}\dot{z}_0^{(1)} - E^{(1)} - E^{(2)}, \\ g_0^{(2)} = (A^{(1)} + A^{(2)})z_0^{(1)} + (B^{(1)} + B^{(2)})\dot{z}_0^{(1)} \\ \quad + \eta^{(1)}(x_0^{(1)} - X) + \xi^{(1)}(\dot{x}_0^{(1)} - \dot{X}) \\ \quad + 2C^{(1)}(z_0^{(1)} - e) + 2D^{(1)}\dot{z}_0^{(1)} + E^{(1)} + E^{(2)} \end{cases} \quad (21)$$

for the stick motion ($\lambda = 0$).

IV. ANALYTICAL CONDITIONS

For the transformation mechanism of the 2-DOF oscillator with strong nonlinearity under a periodic excitation, the switching criteria of stick (or passable) motion and two kinds of grazing motions on dynamic displacement boundaries will be given in the following theorems by using the general theory of flow switchability in Luo [63].

Before developing the switching criteria of motion at discontinuous boundaries, the normal vectors of the discontinuous boundaries should be defined. From the function of the boundary determined in phase space, the normal vector of the separation boundaries in relative frames is defined as

$$\mathbf{n}_{\partial\Omega_{ij}^{(\alpha)}} = \nabla \varphi_{ij}^{(\alpha)} = \left(\frac{\partial \varphi_{ij}^{(\alpha)}}{\partial z^{(\alpha)}}, \frac{\partial \varphi_{ij}^{(\alpha)}}{\partial \dot{z}^{(\alpha)}} \right)^T, \quad (22)$$

where $\nabla = (\partial/\partial z, \partial/\partial \dot{z})^T$ is the Hamilton operator, $i \neq j \in \{0, 1\}$. Considering the fact that the displacement (or stick) boundary $\partial\Omega_{01}^{(\alpha)}$ or $\partial\Omega_{10}^{(\alpha)}$ ($\alpha \in \{(1, 2)\}$) of motion for the mass $m^{(\alpha)}$ ($\alpha \in \{1, 2\}$) is independent on time in relative frames according to (17), thus using (22), we have

$$\mathbf{n}_{\partial\Omega_{10}^{(\alpha)}} = \mathbf{n}_{\partial\Omega_{01}^{(\alpha)}} = (1, 0)^T. \quad (23)$$

Further, the zero-order G-function and first-order G-function for the relative displacement (or stick) boundaries $\partial\Omega_{ij}^{(\alpha)}$ ($i \neq j \in \{0, 1\}$ and $\alpha = 1, 2$) can be expressed

as

$$G_{\partial\Omega_{ij}^{(\alpha)}}^{(0,\lambda)}(\mathbf{z}_\lambda^{(\alpha)}, t_{m\pm}) \equiv G_{\partial\Omega_{ij}^{(\alpha)}}^{(0,\lambda)}(\mathbf{z}_\lambda^{(\alpha)}, \mathbf{x}_\lambda^{(\bar{\alpha})}, t) \Big|_{t=t_{m\pm}} = \mathbf{n}_{\partial\Omega_{ij}^{(\alpha)}}^T \cdot \mathbf{g}_\lambda^{(\alpha)}(\mathbf{z}_\lambda^{(\alpha)}, \mathbf{x}_\lambda^{(\bar{\alpha})}, t) \Big|_{t=t_{m\pm}}, \quad (24)$$

$$G_{\partial\Omega_{ij}^{(\alpha)}}^{(1,\lambda)}(\mathbf{z}_\lambda^{(\alpha)}, t_{m\pm}) \equiv G_{\partial\Omega_{ij}^{(\alpha)}}^{(1,\lambda)}(\mathbf{z}_\lambda^{(\alpha)}, \mathbf{x}_\lambda^{(\bar{\alpha})}, t) \Big|_{t=t_{m\pm}} = \mathbf{n}_{\partial\Omega_{ij}^{(\alpha)}}^T \cdot D\mathbf{g}_\lambda^{(\alpha)}(\mathbf{z}_\lambda^{(\alpha)}, \mathbf{x}_\lambda^{(\bar{\alpha})}, t) \Big|_{t=t_{m\pm}}, \quad (25)$$

where t_m denotes the switching time of the flow $\mathbf{z}_\lambda^{(\alpha)}$ on the corresponding boundary and $t_{m\pm} = t_m \pm 0$ stands for responses in domains rather than on the boundaries.

Using the G-functions and the related theory in Luo [63], the conditions of switchability for stick motion and the two kinds of grazing motions to the boundary are given.

Theorem 1: For the 2-DOF oscillator described in Section 2, if a flow of such system contacts the relative displacement boundary $\partial\Omega_{10}^{(\alpha)}$ ($\alpha \in \{1, 2\}$) at time t_m , the following analytical results hold.

(i) The onset conditions for stick motion of the mass $m^{(1)}$ on the displacement boundary $\partial\Omega_{10}^{(1)}$ at time t_m are guaranteed by

$$\left. \begin{array}{l} \text{either } \dot{z}_1^{(1)}(t_{m-}) > 0 \text{ and } \dot{z}_0^{(1)}(t_{m+}) > 0; \\ \text{or } \left. \begin{array}{l} \dot{z}_1^{(1)}(t_{m-}) = 0 \text{ and } g_1^{(1)}(t_{m-}) > 0, \\ \dot{z}_0^{(1)}(t_{m+}) = 0 \text{ and } g_0^{(1)}(t_{m+}) > 0 \end{array} \right\} \text{ for } \Omega_1^{(1)} \rightarrow \Omega_0^{(1)}. \end{array} \right\} \quad (26)$$

(ii) The onset conditions for stick motion of the mass $m^{(2)}$ on the displacement boundary $\partial\Omega_{10}^{(2)}$ at time t_m are guaranteed by

$$\left. \begin{array}{l} \text{either } \dot{z}_1^{(2)}(t_{m-}) < 0 \text{ and } \dot{z}_0^{(2)}(t_{m+}) < 0; \\ \text{or } \left. \begin{array}{l} \dot{z}_1^{(2)}(t_{m-}) = 0 \text{ and } g_1^{(2)}(t_{m-}) < 0, \\ \dot{z}_0^{(2)}(t_{m+}) = 0 \text{ and } g_0^{(2)}(t_{m+}) < 0 \end{array} \right\} \text{ for } \Omega_1^{(2)} \rightarrow \Omega_0^{(2)}. \end{array} \right\} \quad (27)$$

Proof: The stick motion occurs when the relative displacement of the mass $m^{(1)}$ to the mass $m^{(2)}$ is e at time t_m and is greater than e after time t_m , in other words, the nonstick motion will turn to stick motion during this process. And the essence of this transformation process is the same as the semi-passable flow on the boundary $\partial\Omega_{10}^{(1)}$ as described in systematic theory of flow switchability at separation boundary of [63].

Using the G-functions and decision theorems in Luo [63], the criteria for the appearance of stick motion of the first mass

at $\mathbf{x}_m^{(1)} \in \partial\Omega_{10}^{(1)}$ with time t_m are

$$\left. \begin{array}{l} \text{either } \left. \begin{array}{l} G_{\partial\Omega_{10}^{(1)}}^{(0,1)}(\mathbf{z}_\lambda^{(1)}, t_{m-}) > 0, \\ G_{\partial\Omega_{10}^{(1)}}^{(0,0)}(\mathbf{z}_\lambda^{(1)}, t_{m+}) > 0; \end{array} \right\} \\ G_{\partial\Omega_{10}^{(1)}}^{(0,1)}(\mathbf{z}_\lambda^{(1)}, t_{m-}) = 0 \text{ and } \\ G_{\partial\Omega_{10}^{(1)}}^{(1,1)}(\mathbf{z}_\lambda^{(1)}, t_{m-}) > 0, \\ \text{and} \\ G_{\partial\Omega_{10}^{(1)}}^{(0,0)}(\mathbf{z}_\lambda^{(1)}, t_{m+}) = 0 \text{ and } \\ G_{\partial\Omega_{10}^{(1)}}^{(1,0)}(\mathbf{z}_\lambda^{(1)}, t_{m+}) > 0 \end{array} \right\} \text{ for } \Omega_1^{(1)} \rightarrow \Omega_0^{(1)}. \quad (28)$$

Combined with (18), (23), (24) and (25), the zero-order and first-order G-functions on the relative displacement boundary $\partial\Omega_{10}^{(1)}$ can be computed by

$$G_{\partial\Omega_{10}^{(1)}}^{(0,\lambda)}(\mathbf{z}_\lambda^{(1)}, t_{m\pm}) = \mathbf{n}_{\partial\Omega_{10}^{(1)}}^T \cdot \mathbf{g}_\lambda^{(1)}(\mathbf{z}_\lambda^{(1)}, t_{m\pm}) = \dot{z}_\lambda^{(1)}(t_{m\pm}), \quad (29)$$

$$G_{\partial\Omega_{10}^{(1)}}^{(1,\lambda)}(\mathbf{z}_\lambda^{(1)}, t_{m\pm}) = \mathbf{n}_{\partial\Omega_{10}^{(1)}}^T \cdot D\mathbf{g}_\lambda^{(1)}(\mathbf{z}_\lambda^{(1)}, t_{m\pm}) = g_\lambda^{(1)}(t_{m\pm}), \quad (30)$$

where $\lambda \in \{0, 1\}$.

Integration of (28), (29) and (30) obtains the appearance criteria in (26). In a similar manner, the appearance criteria in (27) holds. \square

Theorem 2: For the 2-DOF oscillator described in Section 2, if a flow of such system contacts the relative displacement boundary $\partial\Omega_{01}^{(\alpha)}$ ($\alpha \in \{1, 2\}$) at time t_m , the following analytical results hold.

(i) For the mass $m^{(1)}$, the vanishing of the stick motion on the displacement boundary $\partial\Omega_{01}^{(1)}$ at time t_m is guaranteed by

$$\left. \begin{array}{l} \text{either } \dot{z}_0^{(1)}(t_{m-}) < 0 \text{ and } \dot{z}_1^{(1)}(t_{m+}) < 0; \\ \text{or } \left. \begin{array}{l} \dot{z}_0^{(1)}(t_{m-}) = 0 \text{ and } g_0^{(1)}(t_{m-}) < 0, \\ \dot{z}_1^{(1)}(t_{m+}) = 0 \text{ and } g_1^{(1)}(t_{m+}) < 0 \end{array} \right\} \text{ for } \Omega_0^{(1)} \rightarrow \Omega_1^{(1)}. \end{array} \right\} \quad (31)$$

(ii) For the mass $m^{(2)}$, the vanishing of the stick motion on the displacement boundary $\partial\Omega_{01}^{(2)}$ at time t_m is guaranteed by

$$\left. \begin{array}{l} \text{either } \dot{z}_0^{(2)}(t_{m-}) > 0 \text{ and } \dot{z}_1^{(2)}(t_{m+}) > 0; \\ \text{or } \left. \begin{array}{l} \dot{z}_0^{(2)}(t_{m-}) = 0 \text{ and } g_0^{(2)}(t_{m-}) > 0, \\ \dot{z}_1^{(2)}(t_{m+}) = 0 \text{ and } g_1^{(2)}(t_{m+}) > 0 \end{array} \right\} \text{ for } \Omega_0^{(2)} \rightarrow \Omega_1^{(2)}. \end{array} \right\} \quad (32)$$

Proof: The stick motions of the masses $m^{(1)}$ and $m^{(2)}$ will vanish when the relative displacement of the mass $m^{(1)}$ to the mass $m^{(2)}$ is equal to e at time t_m and is less than e after time t_m . In other words, the stick motion will turn to nonstick motion during this process, which indicates that this switching mechanism is similar to that of the appearance of stick motion for the mass $m^{(1)}$.

From the non-smooth dynamical theory in Luo [63], the criteria for the vanishing of stick motion of the first mass at $\mathbf{x}_m^{(1)} \in \partial\Omega_{01}^{(1)}$ with time t_m are

$$\left. \begin{aligned} &\text{either } \left. \begin{aligned} G_{\partial\Omega_{01}^{(1)}}^{(0,0)}(\mathbf{z}_\lambda^{(1)}, t_{m-}) < 0, \\ G_{\partial\Omega_{01}^{(1)}}^{(0,1)}(\mathbf{z}_\lambda^{(1)}, t_{m+}) < 0; \\ G_{\partial\Omega_{01}^{(1)}}^{(0,0)}(\mathbf{z}_\lambda^{(1)}, t_{m-}) = 0 \text{ and} \\ G_{\partial\Omega_{01}^{(1)}}^{(1,0)}(\mathbf{z}_\lambda^{(1)}, t_{m-}) < 0, \end{aligned} \right\} \text{for } \Omega_0^{(1)} \rightarrow \Omega_1^{(1)}. \\ &\text{or } \left. \begin{aligned} G_{\partial\Omega_{01}^{(1)}}^{(0,1)}(\mathbf{z}_\lambda^{(1)}, t_{m+}) = 0 \text{ and} \\ G_{\partial\Omega_{01}^{(1)}}^{(1,1)}(\mathbf{z}_\lambda^{(1)}, t_{m+}) < 0 \end{aligned} \right\} \end{aligned} \right\} \quad (33)$$

Therefore, integration of (29), (30) and (33) obtains the criteria for the vanishing of stick motion in (31). Similarly, (32) holds. \square

Theorem 3: For the 2-DOF oscillator described in Section 2, if a flow of such system contacts the relative displacement boundary $\partial\Omega_{10}^{(\alpha)}$ ($\alpha \in \{1, 2\}$) at time t_m , the following analytical results hold.

(i) The necessary and sufficient conditions for the grazing motion of the mass $m^{(1)}$ at displacement boundary $\partial\Omega_{10}^{(1)}$ in nonstick domain $\Omega_1^{(1)}$ at time t_m are

$$\dot{z}_1^{(1)}(t_{m\pm}) = 0 \text{ and } g_1^{(1)}(t_{m\pm}) < 0 \text{ on } \partial\Omega_{10}^{(1)} \text{ in } \Omega_1^{(1)}. \quad (34)$$

(ii) The necessary and sufficient conditions for the grazing motion of the mass $m^{(2)}$ at stick displacement boundary $\partial\Omega_{10}^{(2)}$ in nonstick domain $\Omega_1^{(2)}$ at time t_m are

$$\dot{z}_1^{(2)}(t_{m\pm}) = 0 \text{ and } g_1^{(2)}(t_{m\pm}) > 0 \text{ on } \partial\Omega_{10}^{(2)} \text{ in } \Omega_1^{(2)}. \quad (35)$$

Proof: It is worth noting that grazing at the separation boundary is an important phenomenon in motion transformation mechanism. When the relative displacement $z^{(1)}$ of the mass $m^{(1)}$ to the mass $m^{(2)}$ is e at time t_m , and is less than e before and after time t_m , the grazing motion on the displacement boundary in nonstick domain occurs for the mass $m^{(1)}$. In a same fashion, when the relative displacement $z^{(2)}$ of the mass $m^{(2)}$ to the mass $m^{(1)}$ is $-e$ at time t_m , and is greater than $-e$ before and after time t_m , the grazing motion on the displacement boundary in nonstick domain occurs for the mass $m^{(2)}$.

The grazing flow in nonstick domain is just that the flow in nonstick domain is tangential to the displacement boundary at time t_m and returns back to the nonstick domain after time t_m . Then the criteria for grazing motion at $\mathbf{x}_m^{(1)} \in \partial\Omega_{10}^{(1)}$ with time t_m can be obtained from the discontinuous dynamical theory in Luo [63], i.e.

$$\left. \begin{aligned} G_{\partial\Omega_{10}^{(1)}}^{(0,1)}(\mathbf{z}_\lambda^{(1)}, t_{m\pm}) = 0, \\ G_{\partial\Omega_{10}^{(1)}}^{(1,1)}(\mathbf{z}_\lambda^{(1)}, t_{m\pm}) < 0 \end{aligned} \right\} \text{on } \partial\Omega_{10}^{(1)} \text{ in } \Omega_1^{(1)}. \quad (36)$$

Integration of (29), (30) and (36) proves the criteria of appearance of the grazing motion in free domain in (34). In the same way, (35) are obtained. \square

Theorem 4: For the 2-DOF oscillator described in Section 2, if a flow of such system contacts the relative displacement boundary $\partial\Omega_{01}^{(\alpha)}$ ($\alpha \in \{1, 2\}$) at time t_m , the following analytical results hold.

(i) The appearance conditions for the grazing motion of the mass $m^{(1)}$ on the displacement boundary $\partial\Omega_{01}^{(1)}$ in stick domain $\Omega_0^{(1)}$ at time t_m are

$$\dot{z}_0^{(1)}(t_{m\pm}) = 0 \text{ and } g_0^{(1)}(t_{m\pm}) > 0 \text{ on } \partial\Omega_{01}^{(1)} \text{ in } \Omega_0^{(1)}. \quad (37)$$

(ii) The appearance conditions for the grazing motion of the mass $m^{(2)}$ on the displacement boundary $\partial\Omega_{01}^{(2)}$ in stick domain $\Omega_0^{(2)}$ at time t_m are

$$\dot{z}_0^{(2)}(t_{m\pm}) = 0 \text{ and } g_0^{(2)}(t_{m\pm}) < 0 \text{ on } \partial\Omega_{01}^{(2)} \text{ in } \Omega_0^{(2)}. \quad (38)$$

Proof: As discussed in Theorem 3, the switching process of grazing motion on the separation boundary in the stick domain is as same as that in nonstick domain, however the premise and the criteria of grazing in stick domain may be different. Hence, from Luo [63], the appearance criteria of grazing motion are

$$\left. \begin{aligned} G_{\partial\Omega_{01}^{(1)}}^{(0,0)}(\mathbf{z}_\lambda^{(1)}, t_{m\pm}) = 0, \\ G_{\partial\Omega_{01}^{(1)}}^{(1,0)}(\mathbf{z}_\lambda^{(1)}, t_{m\pm}) > 0 \end{aligned} \right\} \text{on } \partial\Omega_{01}^{(1)} \text{ in } \Omega_0^{(1)}. \quad (39)$$

Combined with (29), (30) and (39), (37) are proved. Similarly, (38) holds. \square

V. MAPPING STRUCTURES AND PERIODIC MOTIONS

To better discuss the stick (or passable) motion, grazing motion and periodic motion with and without stick in the 2-DOF oscillator described in Section 2, the mapping theory will be a useful and efficient method to help us understand all the possible periodic motions of such system, and the mapping structures will be introduced based on the relative displacement boundaries in this section. Thus, the switching sets and the corresponding mappings for motions of each mass will be given primarily, and the four-dimensional mappings for periodic motions in this oscillator system are constituted by the corresponding switching sets and basic mappings. Using such mapping structures, the periodic motions of the two masses will be determined by a group of nonlinear algebraic equations. The basic mappings will be discussed in relative coordinates.

Based on the relative displacement boundaries in (17), the corresponding switching sets of the mass $m^{(\alpha)}$ ($\alpha \in \{1, 2\}$) are expressed by

$$\begin{cases} \sum_{10}^{(1)} = \{(x_k^{(1)}, \dot{x}_k^{(1)}, t_k) | x_k^{(1)} - x_k^{(2)} = e, k \in \mathbb{N}\}, \\ \sum_{10}^{(1)-} = \{(x_k^{(1)}, \dot{x}_k^{(1)}, t_k) | x_k^{(1)} - x_k^{(2)} = e^-, k \in \mathbb{N}\}, \\ \sum_{10}^{(1)+} = \{(x_k^{(1)}, \dot{x}_k^{(1)}, t_k) | x_k^{(1)} - x_k^{(2)} = e^+, k \in \mathbb{N}\}, \end{cases} \quad (40)$$

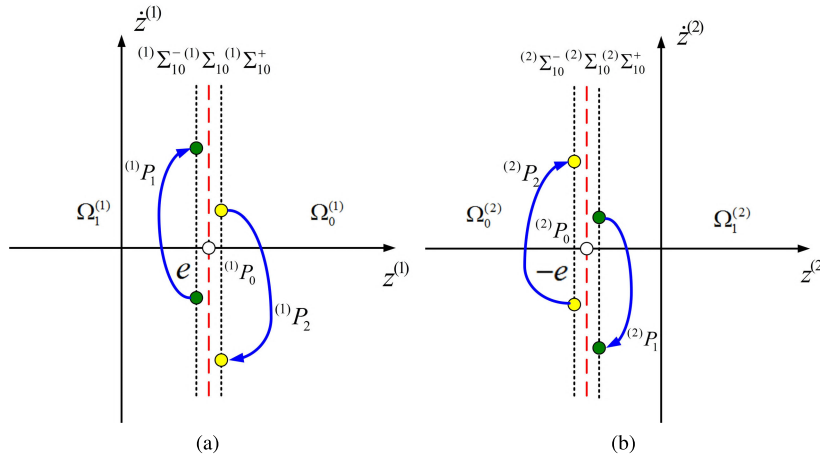


FIGURE 5. Generic mappings in phase space: (a) sub-mappings for the mass $m^{(1)}$ and (b) sub-mappings for the mass $m^{(2)}$.

and

$$\begin{cases} (2) \sum_{10}^- = \{(x_k^{(2)}, \dot{x}_k^{(2)}, t_k) | x_k^{(2)} - x_k^{(1)} = -e, k \in \mathbb{N}\}, \\ (2) \sum_{10}^+ = \{(x_k^{(2)}, \dot{x}_k^{(2)}, t_k) | x_k^{(2)} - x_k^{(1)} = -e^+, k \in \mathbb{N}\}, \\ (2) \sum_{10}^- = \{(x_k^{(2)}, \dot{x}_k^{(2)}, t_k) | x_k^{(2)} - x_k^{(1)} = -e^-, k \in \mathbb{N}\}, \end{cases} \quad (41)$$

where $x_k^{(i)} = x^{(i)}(t_k)$, $\dot{x}_k^{(i)} = \dot{x}^{(i)}(t_k)$ ($i \in \{1, 2\}$) are the displacement and velocity on boundary for the mass $m^{(\alpha)}$ ($\alpha \in \{1, 2\}$) at switching time t_k , accordingly; $e^\pm = \lim_{\varepsilon \rightarrow 0^+} (e \pm \varepsilon)$.

From the above equations, the four-dimensional switching sets of two masses in such oscillator system are further defined as

$$\begin{cases} \sum_{10} = (1) \sum_{10} \otimes (2) \sum_{10} = \{(x_k^{(1)}, \dot{x}_k^{(1)}, x_k^{(2)}, \dot{x}_k^{(2)}, t_k) | \\ x_k^{(1)} - x_k^{(2)} = e, k \in \mathbb{N}\}, \\ \sum_{10}^- = (1) \sum_{10}^- \otimes (2) \sum_{10}^+ = \{(x_k^{(1)}, \dot{x}_k^{(1)}, x_k^{(2)}, \dot{x}_k^{(2)}, t_k) | \\ x_k^{(1)} - x_k^{(2)} = e^-, k \in \mathbb{N}\}, \\ \sum_{10}^+ = (1) \sum_{10}^+ \otimes (2) \sum_{10}^- = \{(x_k^{(1)}, \dot{x}_k^{(1)}, x_k^{(2)}, \dot{x}_k^{(2)}, t_k) | \\ x_k^{(1)} - x_k^{(2)} = e^+, k \in \mathbb{N}\}, \end{cases} \quad (42)$$

where the notation \otimes denotes the direct product of two switching subsets. For the 2-DOF oscillator system described in Section 2, the basic mappings for motions of the two masses $m^{(1)}$ and $m^{(2)}$ are given by

$$P_0 : \sum_{10} \rightarrow \sum_{10}, P_1 : \sum_{10}^- \rightarrow \sum_{10}^-, P_2 : \sum_{10}^+ \rightarrow \sum_{10}^+, \quad (43)$$

where the generic mappings have two components

$$P_0 = ({}^{(1)}P_0, {}^{(2)}P_0)^T, P_1 = ({}^{(1)}P_1, {}^{(2)}P_1)^T, P_2 = ({}^{(1)}P_2, {}^{(2)}P_2)^T \quad (44)$$

and

$$\left. \begin{cases} (i)P_0 : (i) \sum_{10} \rightarrow (i) \sum_{10} \quad \text{for } i = 1, 2, \\ (1)P_1 : (1) \sum_{10}^- \rightarrow (1) \sum_{10}^-, (2)P_1 : (2) \sum_{10}^+ \rightarrow (2) \sum_{10}^+, \\ (1)P_2 : (1) \sum_{10}^+ \rightarrow (1) \sum_{10}^-, (2)P_2 : (2) \sum_{10}^- \rightarrow (2) \sum_{10}^-. \end{cases} \right\} \quad (45)$$

From the above basic mappings, all possible motions including periodic motions in such system can be described through a certain mapping structure and be labeled through such four-dimensional resultant mappings. The generic mappings can be determined in Fig. 5. If the motion lies in free domain $\Omega_1^{(\alpha)}$ (i.e., $x^{(1)} - x^{(2)} < e$), the mapping is plotted by the generic mapping ${}^{(\alpha)}P_1$ ($\alpha \in \{1, 2\}$); if the motion lies in stick domain $\Omega_0^{(\alpha)}$ (i.e., $x^{(1)} - x^{(2)} > e$), the mapping is sketched by the generic mapping ${}^{(\alpha)}P_2$ ($\alpha \in \{1, 2\}$); if the motion reaches to the displacement boundary (i.e., $x^{(1)} - x^{(2)} = e$) and the relative velocity of two objects is zero and this relative motion lasts for a period of time, the generic mapping is presented by ${}^{(\alpha)}P_0$ ($\alpha \in \{1, 2\}$).

Based on the foregoing definitions, the governing equations of displacement and velocity of the two masses $m^{(1)}$ and $m^{(2)}$ for the resultant mapping P_i ($i \in \{0, 1, 2\}$) can be described by a set of four algebraic equations, i.e.

$$\mathbf{f}^{(i)}(\mathbf{m}_k, \mathbf{m}_{k+1}) = 0 \quad \text{for } P_i, \quad (46)$$

with

$$\begin{cases} \mathbf{m}_k = (x_k^{(1)}, \dot{x}_k^{(1)}, x_k^{(2)}, \dot{x}_k^{(2)}, t_k)^T, \\ \mathbf{m}_{k+1} = (x_{k+1}^{(1)}, \dot{x}_{k+1}^{(1)}, x_{k+1}^{(2)}, \dot{x}_{k+1}^{(2)}, t_{k+1})^T, \\ \mathbf{f}^{(i)} = (f_1^{(i)}, f_2^{(i)}, f_3^{(i)}, f_4^{(i)})^T, \end{cases} \quad (47)$$

where

$$\begin{cases} f_1^{(i)}(x_k^{(1)}, \dot{x}_k^{(1)}, x_k^{(2)}, \dot{x}_k^{(2)}, t_k, x_{k+1}^{(1)}, \dot{x}_{k+1}^{(1)}, x_{k+1}^{(2)}, \dot{x}_{k+1}^{(2)}, t_{k+1}) = 0, \\ f_2^{(i)}(x_k^{(1)}, \dot{x}_k^{(1)}, x_k^{(2)}, \dot{x}_k^{(2)}, t_k, x_{k+1}^{(1)}, \dot{x}_{k+1}^{(1)}, x_{k+1}^{(2)}, \dot{x}_{k+1}^{(2)}, t_{k+1}) = 0, \\ f_3^{(i)}(x_k^{(1)}, \dot{x}_k^{(1)}, x_k^{(2)}, \dot{x}_k^{(2)}, t_k, x_{k+1}^{(1)}, \dot{x}_{k+1}^{(1)}, x_{k+1}^{(2)}, \dot{x}_{k+1}^{(2)}, t_{k+1}) = 0, \\ f_4^{(i)}(x_k^{(1)}, \dot{x}_k^{(1)}, x_k^{(2)}, \dot{x}_k^{(2)}, t_k, x_{k+1}^{(1)}, \dot{x}_{k+1}^{(1)}, x_{k+1}^{(2)}, \dot{x}_{k+1}^{(2)}, t_{k+1}) = 0. \end{cases} \quad (48)$$

For analyzing periodic motions in the oscillator system, the symbol for mapping actions is presented as

$$P_{n_k n_{k-1} \dots n_1} = P_{n_k} \circ P_{n_{k-1}} \circ \dots \circ P_{n_1}, \quad (49)$$

where $n_j \in \{0, 1, 2\}$ with $j = 1, 2, \dots, k$.

For instance, consider a generalized mapping structure of a periodic motion with stick in the following

$$P = P_{(2^{k_{m2}} 0^{k_{m0}} 1^{k_{m1}}) \dots (2^{k_{12}} 0^{k_{10}} 1^{k_{11}})} \\ \equiv (P_2^{k_{m2}} \circ P_0^{k_{m0}} \circ P_1^{k_{m1}}) \circ \dots \circ (P_2^{k_{12}} \circ P_0^{k_{10}} \circ P_1^{k_{11}}) \quad (50)$$

where $k_{i\lambda} \in \{0, 1\}$ for $i \in \{1, 2, \dots, m\}$, $\lambda \in \{0, 1, 2\}$ and $P_\lambda^0 = I$.

Define a vector

$$\mathbf{a}_k \equiv (x_k^{(1)}, \dot{x}_k^{(1)}, x_k^{(2)}, \dot{x}_k^{(2)}, t_k)^T. \quad (51)$$

From the previous generalized mapping structure, consider the periodic motion related to the mapping structure in (50) as

$$\mathbf{a}_{k+\sum_{s=1}^m (k_{s2}+k_{s0}+k_{s1})} = P \mathbf{a}_k = P_{(2^{k_{m2}} 0^{k_{m0}} 1^{k_{m1}}) \dots (2^{k_{12}} 0^{k_{10}} 1^{k_{11}})} \mathbf{a}_k. \quad (52)$$

Based on the governing equations in (48), one can obtain a set of nonlinear algebraic equations for such a mapping structure

$$\begin{aligned} \mathbf{f}^{(1)}(\mathbf{a}_k, \mathbf{a}_{k+k_{11}}) &= 0, \\ \mathbf{f}^{(0)}(\mathbf{a}_{k+k_{11}}, \mathbf{a}_{k+k_{11}+k_{10}}) &= 0, \\ \mathbf{f}^{(2)}(\mathbf{a}_{k+k_{11}+k_{10}}, \mathbf{a}_{k+k_{11}+k_{10}+k_{12}}) &= 0, \\ &\dots \dots \\ \mathbf{f}^{(1)}(\mathbf{a}_{k+\sum_{s=1}^{m-1} (k_{s1}+k_{s0}+k_{s2})}, \mathbf{a}_{k+\sum_{s=1}^{m-1} (k_{s1}+k_{s0}+k_{s2})+k_{m1}}) &= 0, \\ \mathbf{f}^{(0)}(\mathbf{a}_{k+\sum_{s=1}^{m-1} (k_{s1}+k_{s0}+k_{s2})+k_{m1}}, \\ &\mathbf{a}_{k+\sum_{s=1}^{m-1} (k_{s1}+k_{s0}+k_{s2})+k_{m1}+k_{m0}}) = 0, \\ \mathbf{f}^{(2)}(\mathbf{a}_{k+\sum_{s=1}^{m-1} (k_{s1}+k_{s0}+k_{s2})+k_{m1}+k_{m0}}, \\ &\mathbf{a}_{k+\sum_{s=1}^m (k_{s1}+k_{s0}+k_{s2})}) = 0. \end{aligned} \quad (53)$$

In addition, the following equations for the periodic motion with such a mapping structure of the two masses need to be satisfied

$$\begin{aligned} x_{k+\sum_{s=1}^m (k_{s2}+k_{s0}+k_{s1})}^{(\alpha)} &= x_k^{(\alpha)}, \\ \dot{x}_{k+\sum_{s=1}^m (k_{s2}+k_{s0}+k_{s1})}^{(\alpha)} &= \dot{x}_k^{(\alpha)}, \\ \Omega t_{k+\sum_{s=1}^m (k_{s2}+k_{s0}+k_{s1})} &= \Omega t_k + 2N\pi, \end{aligned} \quad (54)$$

where N is a positive integer.

Using a similar approach as described above, different periodic motions for the two masses can be discussed as in (50)–(54).

VI. NUMERICAL SIMULATIONS

In this section, numerical results will be presented to better understand the analytic conditions of different motions. From the switching criteria as we discussed in Section 4, the numerical simulations for the switching between the stick and nonstick motions, the occurrence of grazing motion in two different regions and periodic motions for the two masses will be presented in the first subsection by choosing appropriate parameters and initial conditions, as shown in Figs. 6-10. Furthermore, the second subsection will give a comparison of the velocities and accelerations (or forces responses) for the two masses under the two conditions of control force (i.e., desired actuator force) $f(t)$ in Fig. 11, and present the numerical simulation for a periodic motion of this oscillator subjected to control force $f(t) = A_1 \Omega_1^2 \sin(\Omega_1 t)$ in Fig. 12.

A. SIMULATIONS IN THE CASE OF $f(t) = 0$

During simulations, the green dots indicate the starting points of object's movement, and the yellow dots stand for the switching points of motion where the two masses contact the dynamic displacement boundaries. The dynamical responses of the masses $m^{(\alpha)}$ ($\alpha = 1, 2$) are presented in blue and black in Figs. 6-10 (a), (b) and (c), respectively. The dynamic displacement boundaries for the masses $m^{(\alpha)}$ ($\alpha = 1, 2$) are presented by purple and red dashed curves in Figs. 6-10 (a), accordingly. The trajectories of the two masses in relative frames are plotted by black curves, and the relative displacement boundaries are sketched by red dotted lines in Figs. 6-10 (d). The corresponding 1st-order G-functions are described in purple and red in Fig. 7 (f), Fig. 8 (f) and Fig. 10 (f), respectively. The gray regions are the stick domains, and the black arrows stand for the directions of motion of such system in the absolute and relative phase portraits. Figs. 6-10 (g) and (h) describe the corresponding motion switching and the responses of relative displacement with respect to time for the mass $m^{(2)}$ in relative frames.

To demonstrate the switching between the stick and nonstick motions of each mass, the system parameters of the passable motion in such system are considered as $m^{(1)} = 600 \text{ kg}$, $m^{(2)} = 1300 \text{ kg}$, $k_0 = 550 \text{ N/cm}$, $c_0 = 50 \text{ Ncm/s}^2$, $k_1 = 150 \text{ N/cm}$, $c_1 = 6 \text{ Ncm/s}^2$, $k_2 = 490 \text{ N/cm}$, $c_2 = 3 \text{ Ncm/s}^2$, $A = 3 \text{ N}$, $\Omega = 1 \text{ rad/s}$, $e = 3 \text{ cm}$. The initial conditions are chosen as $t_0 = 3 \text{ s}$, $x_0^{(1)} = 4 \text{ cm}$, $\dot{x}_0^{(1)} = 1 \text{ cm/s}$, $x_0^{(2)} = 1 \text{ cm}$, $\dot{x}_0^{(2)} = 2 \text{ cm/s}$. With the above system parameters and initial conditions, the passable motions for each mass are plotted in Fig. 6. At time $t_0 = 3 \text{ s}$, the relative displacement $z^{(1)}$ of the mass $m^{(1)}$ to the mass $m^{(2)}$ is e in Fig. 6 (a) and (d), and the velocities for the masses $m^{(1)}$ and $m^{(2)}$ satisfies $\dot{x}^{(1)} < \dot{x}^{(2)}$ as presented in Fig. 6 (f), which fits the first case of the switching criteria in (31) and (32), therefore, each mass will move away from the displacement boundary after time t_0 and then enter the free region $\Omega_1^{(\alpha)}$ ($\alpha \in \{1, 2\}$). Each mass does free motion until it reach the displacement boundary at time $t_1 = 8.2354 \text{ s}$, which can be observed in Fig. 6 (a) and (d). At this time,

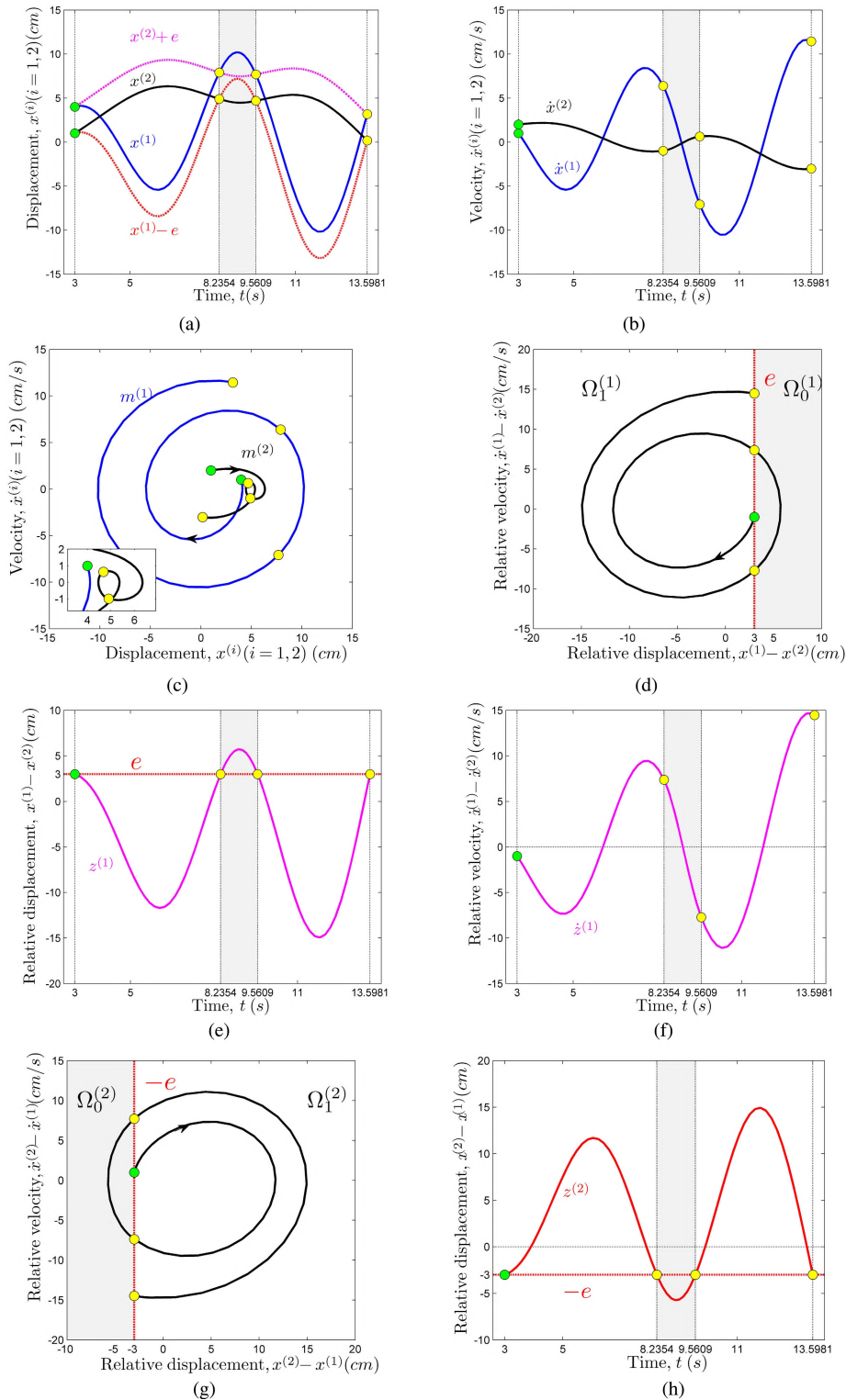


FIGURE 6. Numerical simulation of a passable motion for the two masses: (a) displacement–time history, (b) velocity–time history, (c) phase trajectory, (d) and (g) phase trajectory in relative coordinate, (e) and (h) relative displacement–time history, (f) relative velocity–time history ($m^{(1)} = 600 \text{ kg}$, $m^{(2)} = 1300 \text{ kg}$, $k_0 = 550 \text{ N/cm}$, $c_0 = 50 \text{ Ncm/s}^2$, $k_1 = 150 \text{ N/cm}$, $c_1 = 6 \text{ Ncm/s}^2$, $k_2 = 490 \text{ N/cm}$, $c_2 = 3 \text{ Ncm/s}^2$, $A = 3 \text{ N}$, $\Omega = 1 \text{ rad/s}$, $e = 3 \text{ cm}$). The initial conditions are $t_0 = 3 \text{ s}$, $x^{(1)} = 4 \text{ cm}$, $\dot{x}^{(1)} = 1 \text{ cm/s}$, $x^{(2)} = 1 \text{ cm}$, $\dot{x}^{(2)} = 2 \text{ cm/s}$.

the relative velocity $\dot{z}^{(1)} > 0$ as we observed in Fig. 6 (f) (i.e., $\dot{x}^{(1)} > \dot{x}^{(2)}$ in Fig. 6 (b)), so the first case of the switching

conditions in (26) and (27) in Theorem 1 are fitted, thus each mass will cross the displacement boundary $\partial\Omega_{10}^{(\alpha)}$ at

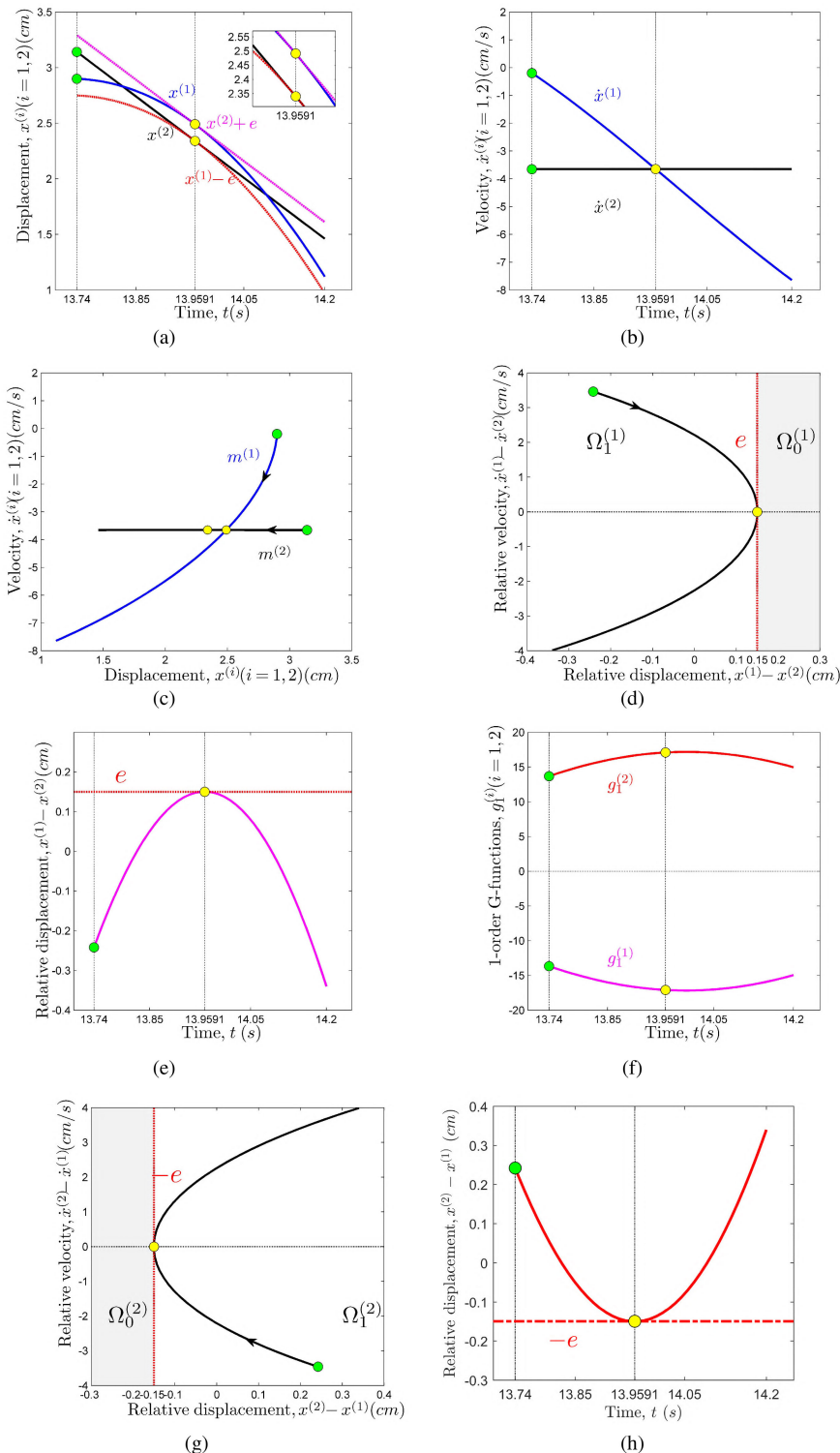


FIGURE 7. Numerical simulation of a grazing motion for the two masses: (a) displacement–time history, (b) velocity–time history, (c) phase trajectory, (d) and (g) phase trajectory in relative coordinate, (e) and (h) relative displacement–time history, (f) 1-order G-function–time history ($m^{(1)} = 156 \text{ kg}$, $m^{(2)} = 1000 \text{ kg}$, $k_0 = 570 \text{ N/cm}$, $c_0 = 66.7 \text{ Ncm/s}^2$, $k_1 = 160 \text{ N/cm}$, $c_1 = 6.28 \text{ Ncm/s}^2$, $k_2 = 486 \text{ N/cm}$, $c_2 = 2.5 \text{ Ncm/s}^2$, $A = 5 \text{ N}$, $\Omega = 1.6 \text{ rad/s}$, $e = 0.15 \text{ cm}$). The initial conditions are $t_0 = 13.74 \text{ s}$, $x^{(1)} = 2.8991 \text{ cm}$, $\dot{x}^{(1)} = -0.1969 \text{ cm/s}$, $x^{(2)} = 3.1411 \text{ cm}$, $\dot{x}^{(2)} = -3.6552 \text{ cm/s}$.

time t_1 and enter the stick domain $\Omega_0^{(\alpha)}$ ($\alpha \in \{1, 2\}$) after time t_1 . From Fig. 6 (e), each mass moves in stick domain

$\Omega_0^{(\alpha)}$ ($\alpha \in \{1, 2\}$) until time $t_2 = 9.5609 \text{ s}$. At time t_2 , each mass reaches the displacement boundary $\partial\Omega_0^{(\alpha)}$ ($\alpha \in \{1, 2\}$)

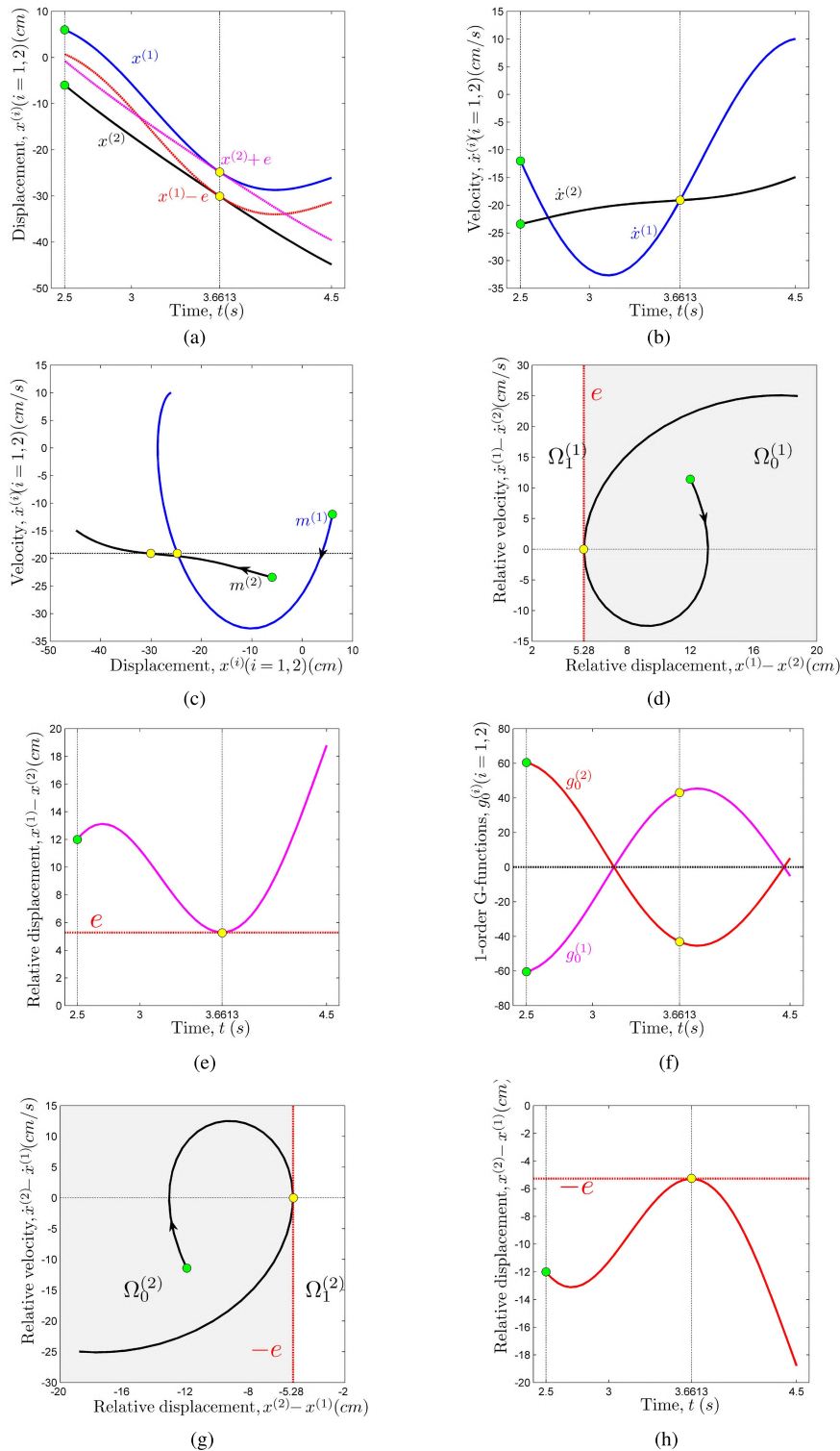


FIGURE 8. Numerical simulation of a grazing motion for the two masses: (a) displacement–time history, (b) velocity–time history, (c) phase trajectory, (d) and (g) phase trajectory in relative coordinate, (e) and (h) relative displacement–time history, (f) 1-order G-function–time history ($m^{(1)} = 50 \text{ kg}$, $m^{(2)} = 240 \text{ kg}$, $k_0 = 70 \text{ N/cm}$, $c_0 = 13 \text{ Ncm/s}^2$, $k_1 = 75 \text{ N/cm}$, $c_1 = 8 \text{ Ncm/s}^2$, $k_2 = 50 \text{ N/cm}$, $c_2 = 4 \text{ Ncm/s}^2$, $A = 15 \text{ N}$, $\Omega = 1.8 \text{ rad/s}$, $e = 5.28 \text{ cm}$). The initial conditions are $t_0 = 2.5 \text{ s}$, $x^{(1)} = 6 \text{ cm}$, $\dot{x}^{(1)} = -12 \text{ cm/s}$, $x^{(2)} = -6 \text{ cm}$, $\dot{x}^{(2)} = -23.41 \text{ cm/s}$.

(i.e., $x^{(1)} - x^{(2)} = e$) with the relative velocity $\dot{z}^{(1)} < 0$ as presented in Fig. 6 (a), (d) and (f), by Theorem 2, each mass

will move freely in domain $\Omega_1^{(\alpha)}$ ($\alpha \in \{1, 2\}$) until switching time $t_3 = 13.5981 \text{ s}$. In addition, the motion switching of a

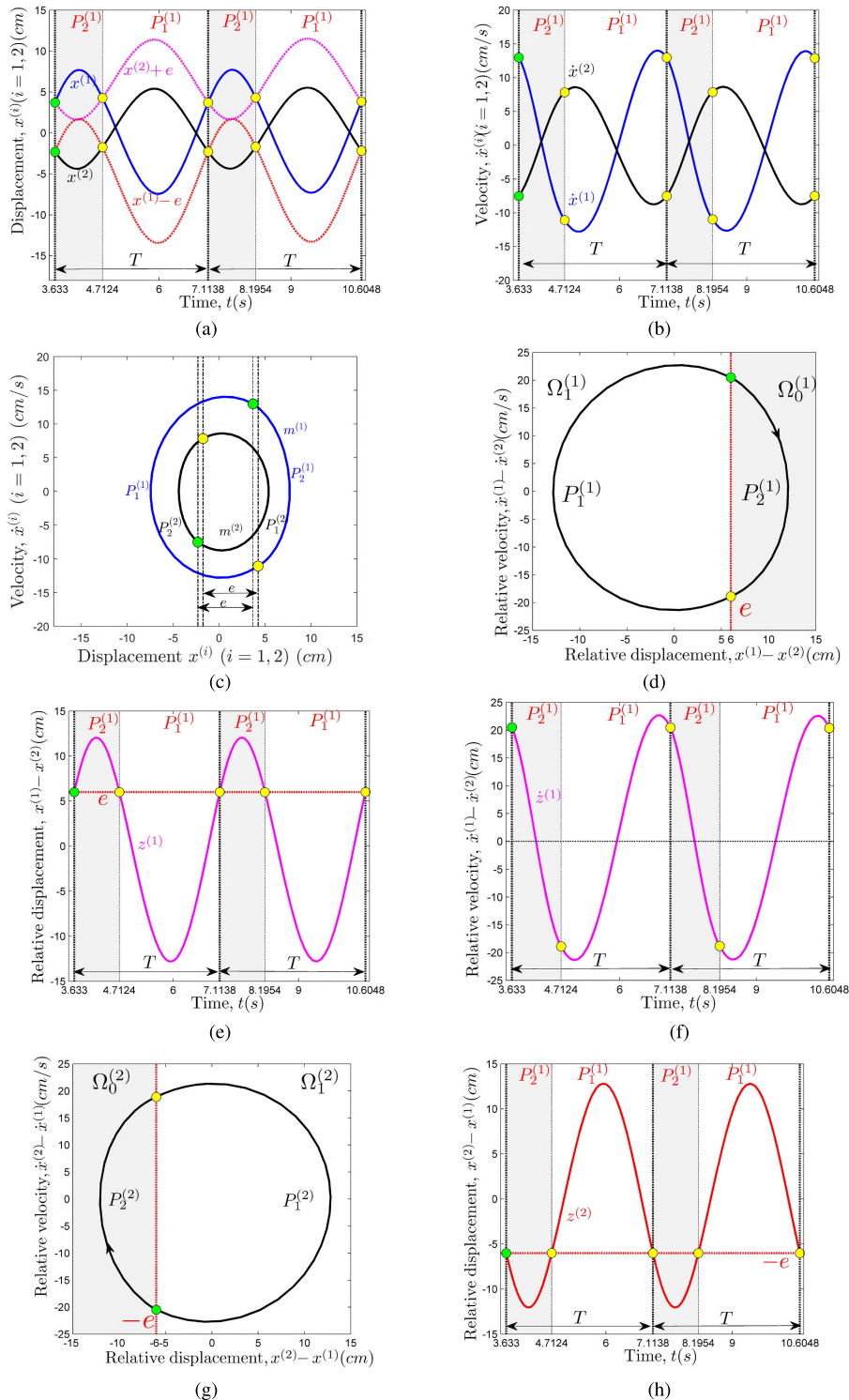


FIGURE 9. Numerical simulation of a periodic passable motion for the two masses: (a) displacement–time history, (b) velocity–time history, (c) phase trajectory, (d) and (g) phase trajectory in relative coordinate, (e) and (h) relative displacement–time history, (f) 0-order G-function–time history ($m^{(1)} = 60 \text{ kg}$, $m^{(2)} = 130 \text{ kg}$, $k_0 = 50 \text{ N/cm}$, $c_0 = 50 \text{ Ncm/s}^2$, $k_1 = 150 \text{ N/cm}$, $c_1 = 6 \text{ Ncm/s}^2$, $k_2 = 90 \text{ N/cm}$, $c_2 = 5 \text{ Ncm/s}^2$, $A = 13 \text{ N}$, $\Omega = 1.8 \text{ rad/s}$, $e = 6 \text{ cm}$). The initial conditions are $t_0 = 3.633 \text{ s}$, $x^{(1)} = 3.6978 \text{ cm}$, $\dot{x}^{(1)} = 12.9795 \text{ cm/s}$, $x^{(2)} = -2.3022 \text{ cm}$, $\dot{x}^{(2)} = -7.515 \text{ cm/s}$.

passable motion for such system in relative frames can be also observed in Fig. 6 (d) for the mass $m^{(1)}$ and in Fig. 6 (g) for the mass $m^{(2)}$.

The simulation of a grazing motion in nonstick domain $\Omega_1^{(\alpha)}$ ($\alpha \in \{1, 2\}$) is presented in Fig. 7. The parameters and original conditions are $m^{(1)} = 156 \text{ kg}$, $m^{(2)} = 1000 \text{ kg}$,

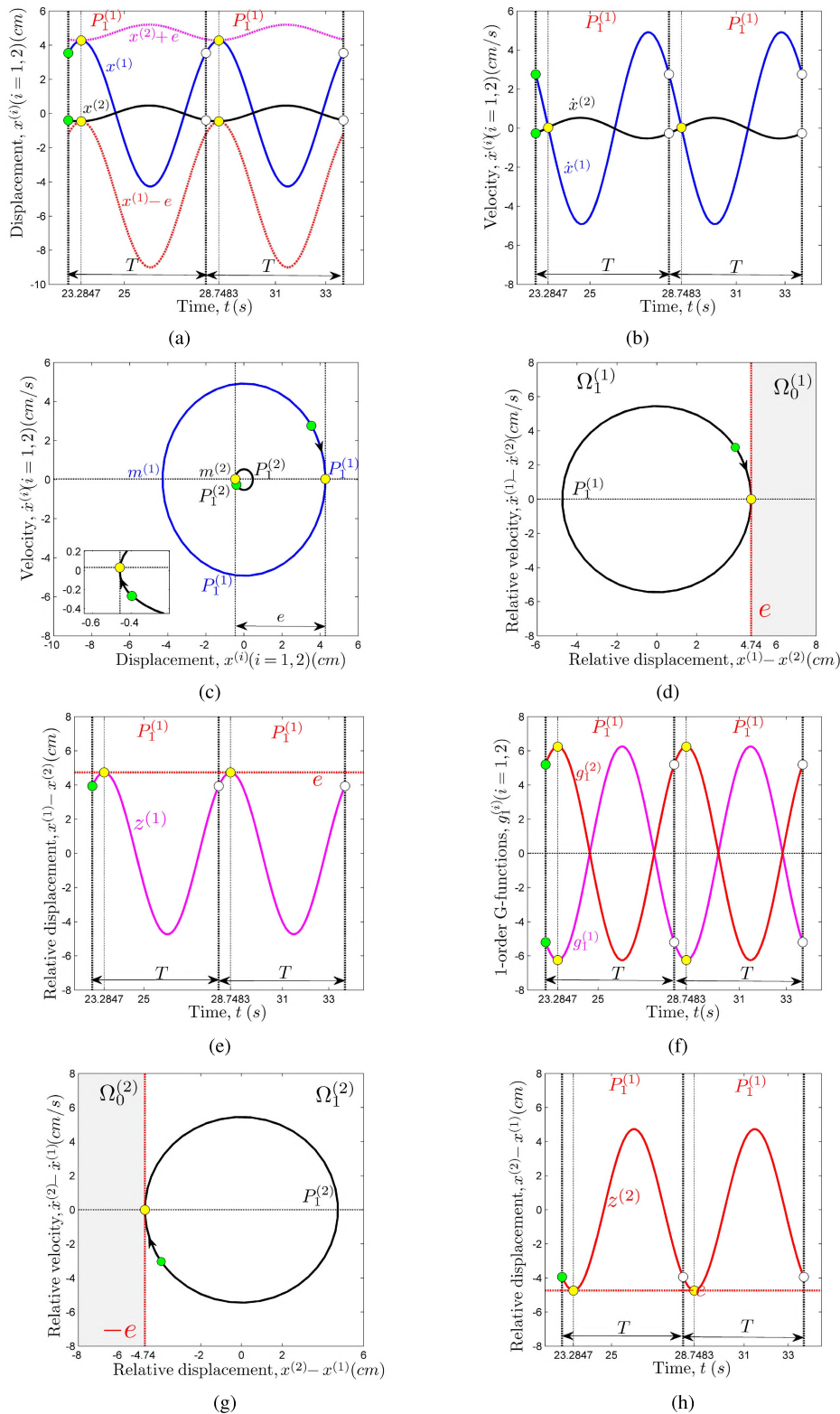


FIGURE 10. Numerical simulation of a periodic grazing motion for the two masses: (a) displacement–time history, (b) velocity–time history, (c) phase trajectory, (d) and (g) phase trajectory in relative coordinate, (e) and (h) relative displacement–time history, (f) 1-order G-function–time history ($m^{(1)} = 256$ kg, $m^{(2)} = 1170$ kg, $k_0 = 560$ N/cm, $c_0 = 60$ Ncm/s², $k_1 = 170$ N/cm, $c_1 = 7.5$ Ncm/s², $k_2 = 437$ N/cm, $c_2 = 3.3$ Ncm/s², $A = 3$ N, $\Omega = 1.15$ rad/s, $e = 4.74$ cm). The initial conditions are $t_0 = 22.7720$ s, $x^{(1)} = 3.5402$ cm, $\dot{x}^{(1)} = 2.7615$ cm/s, $x^{(2)} = -0.3968$ cm, $\dot{x}^{(2)} = -0.2667$ cm/s.

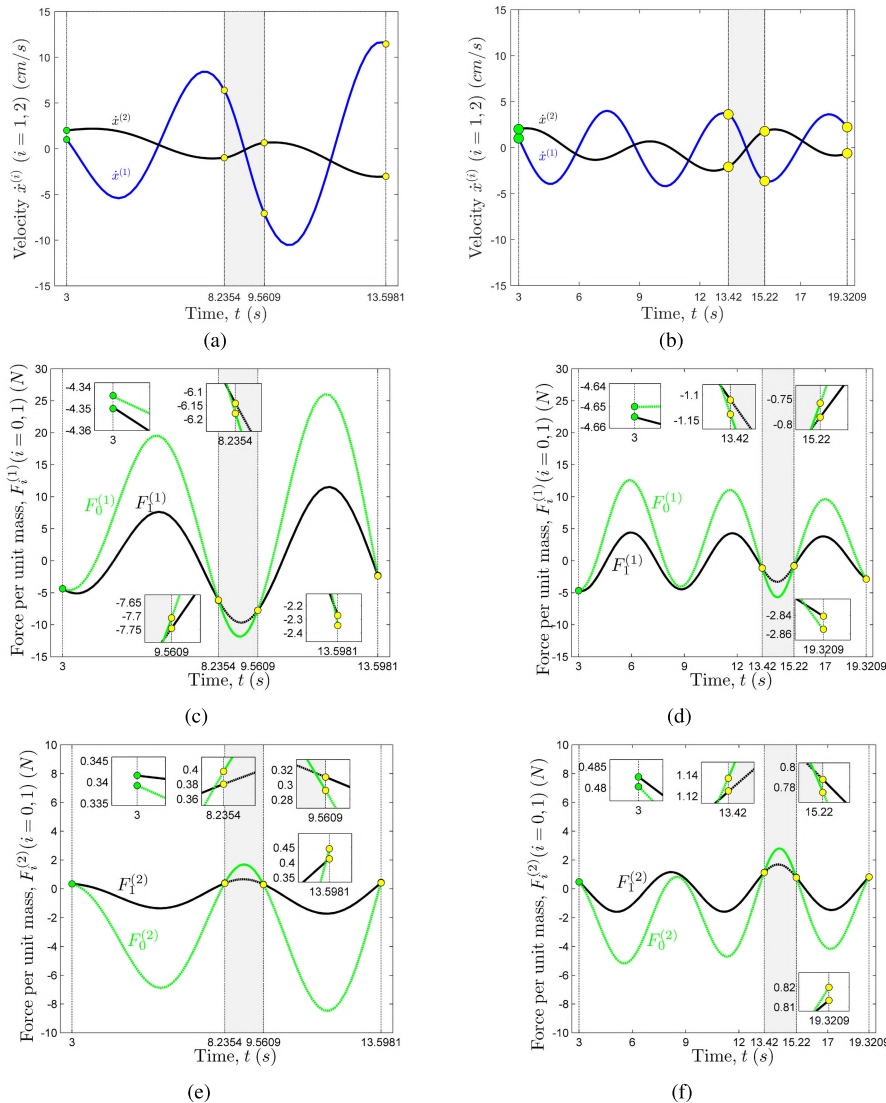


FIGURE 11. Numerical simulation of a stick motion: (a) and (b) velocity–time history for the two masses, (c) and (d) Forces–time history for the mass $m^{(1)}$, (e) and (f) Forces–time history for the mass $m^{(2)}$, ($m^{(1)} = 600 \text{ kg}$, $m^{(2)} = 1300 \text{ kg}$, $k_0 = 550 \text{ N/cm}$, $c_0 = 50 \text{ Ncm/s}^2$, $k_1 = 150 \text{ N/cm}$, $c_1 = 6 \text{ Ncm/s}^2$, $k_2 = 490 \text{ N/cm}$, $c_2 = 3 \text{ Ncm/s}^2$, $A = 3 \text{ N}$, $\Omega = 1 \text{ rad/s}$, $A_1 = 1300 \text{ N}$, $\Omega_1 = 1 \text{ rad/s}$, $e = 3 \text{ cm}$). The initial conditions are $t_0 = 3 \text{ s}$, $x^{(1)} = 4 \text{ cm}$, $\dot{x}^{(1)} = 1 \text{ cm/s}$, $x^{(2)} = 1 \text{ cm}$, $\dot{x}^{(2)} = 2 \text{ cm/s}$.

$k_0 = 570 \text{ N/cm}$, $c_0 = 66.7 \text{ Ncm/s}^2$, $k_1 = 160 \text{ N/cm}$, $c_1 = 6.28 \text{ Ncm/s}^2$, $k_2 = 486 \text{ N/cm}$, $c_2 = 2.5 \text{ Ncm/s}^2$, $A = 5 \text{ N}$, $\Omega = 1.6 \text{ rad/s}$, $e = 0.15 \text{ cm}$ and $t_0 = 13.74 \text{ s}$, $x^{(1)} = 2.8991 \text{ cm}$, $\dot{x}^{(1)} = -0.1969 \text{ cm/s}$, $x^{(2)} = 3.1411 \text{ cm}$, $\dot{x}^{(2)} = -3.6552 \text{ cm/s}$, respectively. For convenience, the start position of such an oscillator is placed in the nonstick domain $\Omega^{(\alpha)}$. When time t satisfies the range of $t \in (t_0, 13.9591 \text{ s})$, each mass moves in the free regions. At time $t_1 = 13.9591 \text{ s}$, the difference of displacement between the masses $m^{(1)}$ and $m^{(2)}$ is e with the relative velocity $\dot{z}^{(1)} > 0$ and G-functions $g_1^{(1)} < 0$, $g_1^{(2)} > 0$, as sketched in Fig. 7 (a), (b) and (f), respectively, which follows the switching criteria of Theorem 3, consequently, each mass tangentially moves back to the nonstick regions when it gets to the displacement boundary. In Fig. 7 (d) and (g), we can see the process visually in relative frames.

Based on (37) in Theorem 4, another grazing motion of each mass in the stick domain $\Omega_0^{(\alpha)}$ ($\alpha \in \{1, 2\}$) can be obtained at time $t = 3.6613 \text{ s}$ in Fig. 8, where the parameters and original conditions are $m^{(1)} = 50 \text{ kg}$, $m^{(2)} = 240 \text{ kg}$, $k_0 = 70 \text{ N/cm}$, $c_0 = 13 \text{ Ncm/s}^2$, $k_1 = 75 \text{ N/cm}$, $c_1 = 8 \text{ Ncm/s}^2$, $k_2 = 50 \text{ N/cm}$, $c_2 = 4 \text{ Ncm/s}^2$, $A = 15 \text{ N}$, $\Omega = 1.8 \text{ rad/s}$, $e = 5.28 \text{ cm}$ and $t_0 = 2.5 \text{ s}$, $x^{(1)} = 6 \text{ cm}$, $\dot{x}^{(1)} = -12 \text{ cm/s}$, $x^{(2)} = -6 \text{ cm}$, $\dot{x}^{(2)} = -23.41 \text{ cm/s}$.

The simulation of a periodic passable motion with two periods ($2T$) is plotted in Fig. 9 with the parameters $m^{(1)} = 60 \text{ kg}$, $m^{(2)} = 130 \text{ kg}$, $k_0 = 50 \text{ N/cm}$, $c_0 = 50 \text{ Ncm/s}^2$, $k_1 = 150 \text{ N/cm}$, $c_1 = 6 \text{ Ncm/s}^2$, $k_2 = 90 \text{ N/cm}$, $c_2 = 5 \text{ Ncm/s}^2$, $A = 13 \text{ N}$, $\Omega = 1.8 \text{ rad/s}$, $e = 6 \text{ cm}$. Using the original conditions as $t_0 = 3.633 \text{ s}$, $x^{(1)} = 3.6978 \text{ cm}$, $\dot{x}^{(1)} = 12.9795 \text{ cm/s}$, $x^{(2)} = -2.3022 \text{ cm}$, $\dot{x}^{(2)} = -7.515 \text{ cm/s}$. As we can see in Fig. 9 (d), the start position of each mass

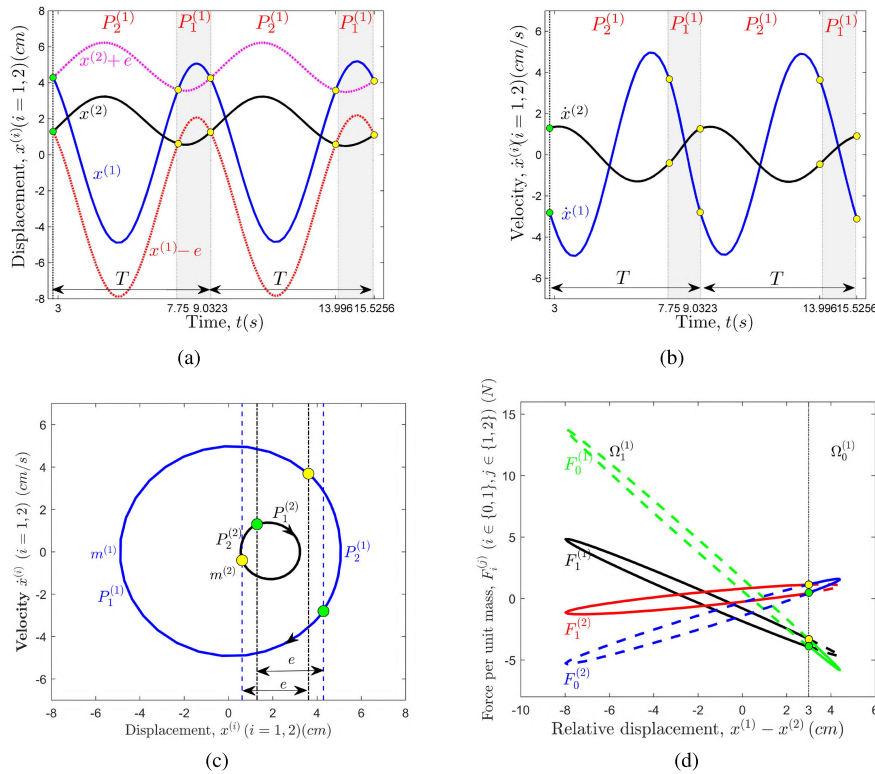


FIGURE 12. Numerical simulation of a periodic stick motion for the two masses: (a) displacement-time history, (b) velocity-time history, (c) phase trajectory, (d) Forces-time history ($m^{(1)} = 600 \text{ kg}$, $m^{(2)} = 1300 \text{ kg}$, $k_0 = 550 \text{ N/cm}$, $c_0 = 50 \text{ Ncm/s}^2$, $k_1 = 50 \text{ N/cm}$, $c_1 = 6 \text{ Ncm/s}^2$, $k_2 = 490 \text{ N/cm}$, $c_2 = 3 \text{ Ncm/s}^2$, $A = 3 \text{ N}$, $\Omega = 1 \text{ rad/s}$, $A_1 = 1300 \text{ N}$, $\Omega_1 = 1 \text{ rad/s}$, $e = 3 \text{ cm}$). The initial conditions are $t_0 = 2.8 \text{ s}$, $x^{(1)} = 4.2907 \text{ cm}$, $\dot{x}^{(1)} = -2.8069 \text{ cm/s}$, $x^{(2)} = 1.2907 \text{ cm}$, $\dot{x}^{(2)} = 1.295 \text{ cm/s}$.

is on the displacement boundaries $\partial\Omega_{01}^{(\alpha)}$ ($\alpha = 1, 2$) in green dots. At time $t_0 = 3.633 \text{ s}$, it follows from Fig. 9 (f) that the relative velocity $\dot{z}^{(1)}$ is greater than zero (i.e., $\dot{x}^{(1)} > \dot{x}^{(2)}$), which satisfies the criteria in (26) and (27) in Theorem 1, thus each mass will cross the displacement boundary and into the stick domain $\Omega_0^{(\alpha)}$ ($\alpha \in \{1, 2\}$). Then, in Fig. 9 (a) and (d), each mass reaches the displacement boundary $\partial\Omega_{01}^{(\alpha)}$ ($\alpha \in \{1, 2\}$) at time $t_1 = 4.7124 \text{ s}$, and in Fig. 9 (e), the relative velocity $\dot{z}^{(1)} < 0$ at time t_1 , which fits Theorem 2, thus each mass will get inter the nonstick domain $\Omega_1^{(\alpha)}$ ($\alpha \in \{1, 2\}$) from the boundary at time t_1 . At time $t_2 = 7.1138 \text{ s}$, each mass reaches to the displacement boundary again, at this points, the position of each mass coincides with the original position. Therefore, the first periodic passable motion for each mass is realized, and the second periodic motion can be also explained and observed. The periodic phase trajectory of each mass in absolute and relative frames can be seen more visually in Fig. 9 (c), (d) or (g), respectively.

In Fig. 10, the parameters are $m^{(1)} = 256 \text{ kg}$, $m^{(2)} = 1170 \text{ kg}$, $k_0 = 560 \text{ N/cm}$, $c_0 = 60 \text{ Ncm/s}^2$, $k_1 = 170 \text{ N/cm}$, $c_1 = 7.5 \text{ Ncm/s}^2$, $k_2 = 437 \text{ N/cm}$, $c_2 = 3.3 \text{ Ncm/s}^2$, $A = 3 \text{ N}$, $\Omega = 1.15 \text{ rad/s}$, $e = 4.74 \text{ cm}$, which is used to achieve a periodic grazing motion for this oscillator in the nonstick region. $t_0 = 22.7720 \text{ s}$, $x^{(1)} = 3.5402 \text{ cm}$, $\dot{x}^{(1)} = 2.7615 \text{ cm/s}$, $x^{(2)} = -0.3968 \text{ cm}$, $\dot{x}^{(2)} = -0.2667 \text{ cm/s}$ are original conditions. During the time interval $(t_0, 23.2847 \text{ s})$,

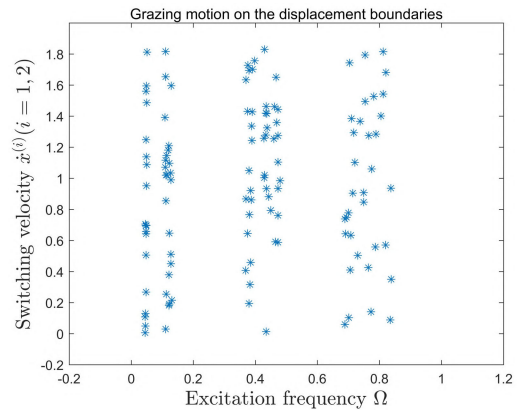


FIGURE 13. Grazing motion on the displacement boundary $\partial\Omega_{ij}^{(2)}$ ($i \neq j \in \{0, 1\}$) ($m^{(1)} = 35 \text{ kg}$, $m^{(2)} = 250 \text{ kg}$, $k_0 = 1600 \text{ N/cm}$, $c_0 = 100 \text{ Ncm/s}^2$, $k_1 = 160 \text{ N/cm}$, $c_1 = 10 \text{ Ncm/s}^2$, $k_2 = 200 \text{ N/cm}$, $c_2 = 3 \text{ Ncm/s}^2$, $A = 3 \text{ N}$, $\Omega = 1 \text{ rad/s}$, $A_1 = 250 \text{ N}$, $\Omega_1 = 1 \text{ rad/s}$, $e = 14.4 \text{ cm}$, $x^{(1)} = 0.6657 \text{ cm}$, $x^{(2)} = -13.7343 \text{ cm/s}$).

each mass moves freely in domain $\Omega_1^{(\alpha)}$ ($\alpha \in \{1, 2\}$) without the effect of the third linear spring and damping. Then in Fig. 10 (b) and (f), each mass contacts the displacement boundary at time $t_1 = 23.2847 \text{ s}$ with the relative velocity $\dot{z}^{(1)} = 0$ and 1st-order G-functions $g_1^{(1)} < 0$ and $g_1^{(2)} > 0$, based on the criteria of Theorem 3, the grazing motion for each mass occurs on displacement boundaries, then each mass moves back to its free domain after this switching

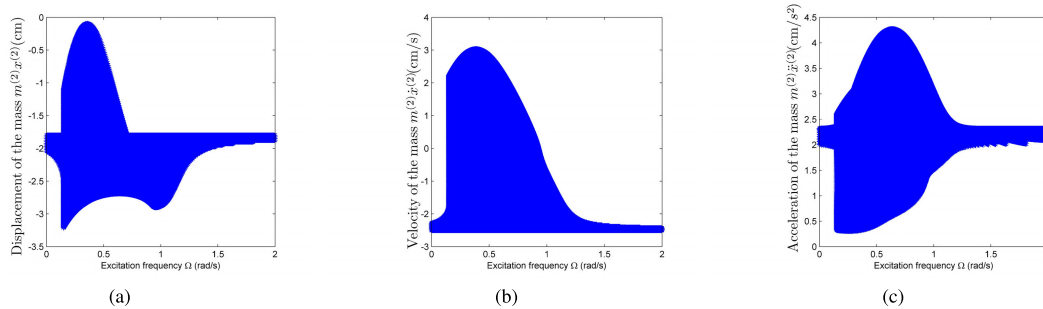


FIGURE 14. Stick scenarios varying with driving frequency ($m^{(1)} = 35 \text{ kg}$, $m^{(2)} = 350 \text{ kg}$, $k_0 = 1600 \text{ N/cm}$, $c_0 = 100 \text{ Ncm/s}^2$, $k_1 = 160 \text{ N/cm}$, $c_1 = 10 \text{ Ncm/s}^2$, $k_2 = 200 \text{ N/cm}$, $c_2 = 3 \text{ Ncm/s}^2$, $A = 3 \text{ N}$, $A_1 = 350 \text{ N}$, $\Omega_1 = 1 \text{ rad/s}$, $e = 3 \text{ cm}$). The initial conditions are $t_0 = 2.2 \text{ s}$, $x^{(1)} = 1.2 \text{ cm}$, $\dot{x}^{(1)} = 1.3 \text{ cm/s}$, $x^{(2)} = -1.8 \text{ cm}$, $\dot{x}^{(2)} = -2.5 \text{ cm/s}$.

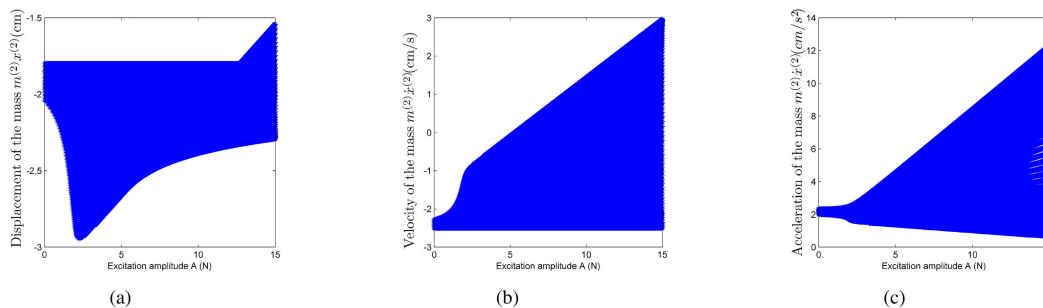


FIGURE 15. Stick scenarios varying with amplitude ($m^{(1)} = 35 \text{ kg}$, $m^{(2)} = 350 \text{ kg}$, $k_0 = 1600 \text{ N/cm}$, $c_0 = 100 \text{ Ncm/s}^2$, $k_1 = 160 \text{ N/cm}$, $c_1 = 10 \text{ Ncm/s}^2$, $k_2 = 200 \text{ N/cm}$, $c_2 = 3 \text{ Ncm/s}^2$, $\Omega = 1 \text{ rad/s}$, $A_1 = 350 \text{ N}$, $\Omega_1 = 1 \text{ rad/s}$, $e = 3 \text{ cm}$). The initial conditions are $t_0 = 2.2 \text{ s}$, $x^{(1)} = 1.2 \text{ cm}$, $\dot{x}^{(1)} = 1.3 \text{ cm/s}$, $x^{(2)} = -1.8 \text{ cm}$, $\dot{x}^{(2)} = -2.5 \text{ cm/s}$.

time t_1 . After that, the position of each mass coincides with the original position at time $t_2 = 28.2356 \text{ s}$. The second periodic motion can be also explained and observed. The periodic phase trajectory of each masses in absolute and relative frames can be seen more visually in Fig. 10 (c), (d) or (g), respectively.

B. SIMULATIONS IN THE CASE OF $f(t) = A_1 \Omega_1^2 \sin(\Omega_1 t)$

In this subsection, the effect of the control force $f(t)$ on the velocity and acceleration of two masses is studied through a set of comparison graphs in Fig. 11. Based on the same system parameters as shown in Fig. 6, $A_1 = 1300 \text{ N}$ and $\Omega_1 = 1 \text{ rad/s}$ are selected to present stick motions of the two masses. The time histories of velocities, acceleration (i.e., force of per unit mass) of the mass $m^{(1)}$ and the mass $m^{(2)}$ are plotted in Fig. 11 (a), (c), (e) with the control force $f(t) = 0$ and in Fig. 11 (b), (d), (f) with the control force $f(t) = A_1 \Omega_1^2 \sin(\Omega_1 t)$, respectively. The black curves and green curves denote the force’s responses of the two masses in free domains and stick domains, respectively. By comparing Fig. 11 (a) and (b), (c) and (d), (e) and (f), it can be clearly seen that the amplitudes of velocity and acceleration for the two masses with $f(t) = A_1 \Omega_1^2 \sin(\Omega_1 t)$ are much smaller than those with $f(t) = 0$. Therefore, the vibration amplitudes of the two masses can be reduced through appropriate control force generated by the control unit of system or exerted by the external excitation, which means that the stability and comfort of the vehicle can be improved by the control force.

Choosing the same parameters as Fig. 11, $k_1 = 50 \text{ N/cm}$ is used to demonstrate a periodic passable motion for each

mass in Fig. 12. $t_0 = 2.8 \text{ s}$, $x^{(1)} = 4.2907 \text{ cm}$, $\dot{x}^{(1)} = -2.8069 \text{ cm/s}$, $x^{(2)} = 1.2907 \text{ cm}$, $\dot{x}^{(2)} = 1.295 \text{ cm/s}$ are original conditions.

VII. STICK AND BIFURCATION SCENARIOS FOR DRIVING FREQUENCY OR AMPLITUDE

For the purpose of investigating stick motion and giving a reference for selecting appropriate parameters in such a 2-DOF oscillator, stick and bifurcation scenarios varying with driving frequency or amplitude will be presented in this section.

For obtaining a grazing motion on the displacement boundaries $\partial\Omega_{10}^{(2)}$ and $\partial\Omega_{01}^{(2)}$, the criteria in Theorem 3 and Theorem 4 are used in this computer program. The parameters are $m^{(1)} = 35 \text{ kg}$, $m^{(2)} = 250 \text{ kg}$, $k_0 = 1600 \text{ N/cm}$, $c_0 = 100 \text{ Ncm/s}^2$, $k_1 = 160 \text{ N/cm}$, $c_1 = 10 \text{ Ncm/s}^2$, $k_2 = 200 \text{ N/cm}$, $c_2 = 3 \text{ Ncm/s}^2$, $A = 3 \text{ N}$, $\Omega = 1 \text{ rad/s}$, $A_1 = 250 \text{ N}$, $\Omega_1 = 1 \text{ rad/s}$, $e = 14.4 \text{ cm}$, $x^{(1)} = 0.6657 \text{ cm}$, $x^{(2)} = -13.7343 \text{ cm/s}$. The two masses have the same velocity when they graze on the separation boundary. Thus, switching velocity of the two masses on the displacement boundary versus excitation frequency in a bifurcation scenario is presented in Fig. 13 in the range of $\Omega \in [0, 1]$.

To further discuss the stick motion of such oscillator, the displacement, velocity and acceleration of stick motion for the mass $m^{(2)}$ versus frequency and amplitude are given in Figs. 14 and 15 in the range of $\Omega \in [0, 2]$ and $A \in [0, 15]$, respectively. The parameters are $m^{(1)} = 35 \text{ kg}$, $m^{(2)} = 350 \text{ kg}$, $k_0 = 1600 \text{ N/cm}$, $c_0 = 100 \text{ Ncm/s}^2$, $k_1 = 160 \text{ N/cm}$, $c_1 = 10 \text{ Ncm/s}^2$, $k_2 = 200 \text{ N/cm}$, $c_2 = 3 \text{ Ncm/s}^2$, $A_1 = 350 \text{ N}$,

$\Omega_1 = 1 \text{ rad/s}$, $e = 3 \text{ cm}$. And the original conditions are selected as $t_0 = 2.2 \text{ s}$, $x^{(1)} = 1.2 \text{ cm}$, $\dot{x}^{(1)} = 1.3 \text{ cm/s}$, $x^{(2)} = -1.8 \text{ cm}$, $\dot{x}^{(2)} = -2.5 \text{ cm/s}$.

In the future, more numerical simulations and bifurcation scenarios about different parameters will be further analyzed.

VIII. CONCLUSION

In present paper, the discontinuous dynamical behaviors in a class of strongly nonlinear 2-DOF oscillators were discussed. The switching criteria between the stick and nonstick motions and the analytical conditions for the grazing motion to occur in two different regions were developed by means of the G-functions and switching control laws. The discontinuous boundaries of the system configurations were defined and the mapping between these boundaries was formulated. The periodic motions for this oscillator were described via employing the mapping theory. Especially, the stick motions, two kinds of grazing motions and periodic motions for this system were further predicted analytically and simulated numerically. The comparison of the velocities and accelerations (or force's responses) for the two masses under the two conditions of control force was presented, and the results showed that the stability and comfort of the vehicle can be improved by the control force, which is generated by the control unit of system or exerted by the external excitation. In addition, the stick and bifurcation scenarios varying with driving frequency or amplitude were further given to better demonstrate the dynamical behaviors in such system. This paper may provide useful information for parameter selection of vibration systems with clearance, and it also has important reference value for practical applications in other industries or machinery with elastic impacts. The results of this paper can be also extended to a broader class of dynamic systems, such as vibration system with higher than two degrees of freedom and mechanical oscillators with variable damping and stiffness properties.

REFERENCES

- [1] M. V. Blundell, "The influence of rubber bush compliance on vehicle suspension movement," *Mater. Des.*, vol. 19, nos. 1–2, pp. 29–37, Feb. 1998.
- [2] M. Kurimoto and T. Yoshimura, "Active suspension of passenger cars using sliding mode controllers (based on reduced models)," *Int. J. Vehicle Des.*, vol. 19, no. 4, pp. 402–414, Jan. 1998.
- [3] C. Kim and P. I. Ro, "A sliding mode controller for vehicle active suspension systems with non-linearities," *Proc. Inst. Mech. Eng., D, J. Automobile Eng.*, vol. 212, no. 2, pp. 79–92, Feb. 1998.
- [4] N.-C. Shieh, C.-L. Lin, Y.-C. Lin, and K.-Z. Liang, "Optimal design for passive suspension of a light rail vehicle using constrained multiobjective evolutionary search," *J. Sound Vib.*, vol. 285, nos. 1–2, pp. 407–424, Jul. 2005.
- [5] Y.-S. Wu and Y.-B. Yang, "Steady-state response and riding comfort of trains moving over a series of simply supported bridges," *Eng. Struct.*, vol. 25, no. 2, pp. 251–265, Jan. 2003.
- [6] A. Karlström and A. Boström, "An analytical model for train-induced ground vibrations from railways," *J. Sound Vib.*, vol. 292, nos. 1–2, pp. 221–241, Apr. 2006.
- [7] E. Gottzein and B. Lange, "Magnetic suspension control systems for the MBB high speed train," *Automatica*, vol. 11, no. 3, pp. 271–284, May 1975.
- [8] H. Sayyaadi and N. Shokouhi, "A new model in rail-vehicles dynamics considering nonlinear suspension components behavior," *Int. J. Mech. Sci.*, vol. 51, no. 3, pp. 222–232, Mar. 2009.
- [9] S.-H. Ju and H.-T. Lin, "Experimentally investigating finite element accuracy for ground vibrations induced by high-speed trains," *Eng. Struct.*, vol. 30, no. 3, pp. 733–746, Mar. 2008.
- [10] T. Gillespie, *Fundamentals of Vehicle Dynamics*. Warrendale, PA, USA: Society of Automotive Engineers, 1992.
- [11] J. Dixon and Tires, *Suspension and Handling*. Warrendale, PA, USA: Society of Automotive Engineers, 1996.
- [12] S. G. Foda, "Fuzzy control of a quarter-car suspension system," in *Proc. 12th Int. Conf. Microelectron.*, Nov. 2000, pp. 231–234.
- [13] A. E. Baurnal, J. J. McPhee, and P. H. Calamai, "Application of genetic algorithms to the design optimization of an active vehicle suspension system," *Comput. Methods Appl. Mech. Eng.*, vol. 163, nos. 1–4, pp. 87–94, Sep. 1998.
- [14] A. Aly and F. Salem, "Vehicle suspension systems control: A review, international journal of control," *Autom. Syst.*, vol. 2, no. 2, pp. 2165–8285, 2013.
- [15] J. Hartog, "Forced vibrations with combined viscous and Coulomb damping," *Phil. Mag.*, vol. 9, no. 59, pp. 801–817, 1930.
- [16] E. Levitan, "Forced oscillation of a spring-mass system having combined Coulomb and viscous damping," *J. Acoust. Soc. Amer.*, vol. 32, no. 10, pp. 1265–1269, Jan. 1960.
- [17] S. F. Masri, "Electric-analog studies of impact dampers," *Exp. Mech.*, vol. 7, no. 2, pp. 49–55, Feb. 1967.
- [18] J. M. T. Thompson and R. Ghaffari, "Chaos after period-doubling bifurcations in the resonance of an impact oscillator," *Phys. Lett. A*, vol. 91, no. 1, pp. 5–8, Aug. 1982.
- [19] J. Thompson, "Complex dynamics of compliant off-shore structures," *Proc. Roy. Soc. London A, Math. Phys. Sci.*, vol. 387, pp. 407–427, Jun. 1983.
- [20] S. W. Shaw and P. J. Holmes, "A periodically forced piecewise linear oscillator," *J. Sound Vib.*, vol. 90, no. 1, pp. 129–155, Sep. 1983.
- [21] S. W. Shaw and P. J. Holmes, "A periodically forced impact oscillator with large dissipation," *J. Appl. Mech.*, vol. 50, no. 4a, pp. 849–857, Dec. 1983.
- [22] A. Filippov, "Differential equations with discontinuous right-hand side," *Amer. Math. Soc. Transl.*, vol. 2, no. 42, pp. 199–231, 1964.
- [23] A. Filippov, *Differential Equations With Discontinuous Righthand Sides*. Dordrecht, The Netherlands: Kluwer, 1988.
- [24] R. Leine and H. Nijmeijer, *Dynamics and Bifurcations of Non-Smooth Mechanical Systems* (Lecture Notes in Applied and Computational Mechanics), no. 18. Berlin, Germany: Springer-Verlag, 2004.
- [25] M. Bernardo, *Piecewise-Smooth Dynamical Systems: Theory and Applications*. Berlin, Germany: Springer, 2008.
- [26] B. Brogliato, *Nonsmooth Impact Mechanics: Models, Dynamics, and Control*. London, U.K.: Springer, 1996.
- [27] B. Brogliato, *Impacts in Mechanical Systems-Analysis and Modelling* (Lecture Notes in Physics). New York, NY, USA: Springer-Verlag, 2000.
- [28] B. Brogliato, "Some perspectives on the analysis and control of complementarity systems," *IEEE Trans. Autom. Control*, vol. 48, no. 6, pp. 918–935, Jun. 2003.
- [29] V. Acary and B. Brogliato, *Numerical Methods for Nonsmooth Dynamical Systems*. Berlin, Germany: Springer, 2008.
- [30] S. Shaw and B. Balachandran, "A review of nonlinear dynamics of mechanical systems in year 2008," *Jpn. Soc. Mech. Eng.*, vol. 2, no. 3, pp. 611–640, Apr. 2008.
- [31] G. C. K. Yeh, "Forced vibrations of a two-degree-of-freedom system with combined Coulomb and viscous damping," *J. Acoust. Soc. Amer.*, vol. 39, no. 1, pp. 14–24, Jan. 1966.
- [32] A. Zbiciak and Z. Kozyra, "Dynamic analysis of a soft-contact problem using viscoelastic and fractional-elastic rheological models," *Arch. Civil Mech. Eng.*, vol. 15, no. 1, pp. 286–291, Jan. 2015.
- [33] B. Balachandran and A. H. Nayfeh, "Nonlinear motions of beam-mass structure," *Nonlinear Dyn.*, vol. 1, no. 1, pp. 39–61, Jan. 1990.
- [34] B. Balachandran, M.-X. Zhao, and Y.-Y. Li, "Dynamics of elastic structures subjected to impact excitations," *Appl. Nonlinear Chaotic Dyn. Mech.*, vol. 63, pp. 263–272, Jul. 1997.
- [35] B. Balachandran, "Dynamics of an elastic structure excited by harmonic and aharmonic impactor motions," *J. Vib. Control*, vol. 9, nos. 3–4, pp. 265–279, Mar. 2003.
- [36] B. Balachandran, "Nonlinear dynamics of milling processes," *Phil. Trans. Roy. Soc. A, Math. Phys. Eng. Sci.*, vol. 359, pp. 793–819, Apr. 2001.
- [37] P. Flores, J. Ambrósio, and J. P. Claro, "Dynamic analysis for planar multibody mechanical systems with lubricated joints," *Multibody Syst. Dyn.*, vol. 12, no. 1, pp. 47–74, Aug. 2004.

- [38] S. T. Morais, P. Flores, and J. C. P. Claro, "Development of a biomechanical spine model for dynamic analysis," in *Proc. IEEE 2nd Portuguese Meeting Bioeng. (ENBENG)*, Feb. 2012, pp. 1–2.
- [39] E. Askari, P. Flores, D. Dabirrahmani, and R. Appleyard, "Study of the friction-induced vibration and contact mechanics of artificial hip joints," *Tribol. Int.*, vol. 70, pp. 1–10, Feb. 2014.
- [40] B. Blazejczyk-Okolewska, K. Czolczynski, and T. Kapitaniak, "Hard versus soft impacts in oscillatory systems modeling," *Commun. Nonlinear Sci. Numer. Simul.*, vol. 15, no. 5, pp. 1358–1367, May 2010.
- [41] J. P. Chávez, P. Brzeski, and P. Perlikowski, "Bifurcation analysis of nonlinear oscillators interacting via soft impacts," *Int. J. Non-Linear Mech.*, vol. 92, pp. 76–83, Jun. 2017.
- [42] Y. Ma, M. Agarwal, and S. Banerjee, "Border collision bifurcations in a soft impact system," *Phys. Lett. A*, vol. 354, no. 4, pp. 281–287, Jun. 2006.
- [43] J. Ing, E. Pavlovskaia, M. Wiercigroch, and S. Banerjee, "Experimental study of impact oscillator with one-sided elastic constraint," *Philos. Trans. Roy. Soc. A, Math., Phys. Eng. Sci.*, vol. 366, no. 1866, pp. 679–704, Mar. 2008.
- [44] Y. Ma, J. Ing, S. Banerjee, M. Wiercigroch, and E. Pavlovskaia, "The nature of the normal form map for soft impacting systems," *Int. J. Non-Linear Mech.*, vol. 43, no. 6, pp. 504–513, Jul. 2008.
- [45] Y. Yue and J. H. Xie, "Symmetry and bifurcations of a two-degree-of-freedom vibro-impact system," *J. Sound Vib.*, vol. 314, nos. 1–2, pp. 228–245, Jul. 2008.
- [46] Y. Liu, Q. Wang, and H. Xu, "Bifurcations of periodic motion in a three-degree-of-freedom vibro-impact system with clearance," *Commun. Nonlinear Sci. Numer. Simul.*, vol. 48, pp. 1–17, Jul. 2017.
- [47] X. Li, X. Yang, and T. Huang, "Persistence of delayed cooperative models: Impulsive control method," *Appl. Math. Comput.*, vol. 342, pp. 130–146, Feb. 2019.
- [48] X. Li, J. Shen, and R. Rakkiyappan, "Persistent impulsive effects on stability of functional differential equations with finite or infinite delay," *Appl. Math. Comput.*, vol. 329, pp. 14–22, Jul. 2018.
- [49] X. Yang, X. Li, Q. Xi, and P. Duan, "Review of stability and stabilization for impulsive delayed systems," *Math. Biosci. Eng.*, vol. 15, no. 6, pp. 1495–1515, Dec. 2018.
- [50] X. Xu, H. Li, Y. Li, and F. E. Alsaadi, "Output tracking control of Boolean control networks with impulsive effects," *Math. Methods Appl. Sci.*, vol. 41, no. 4, pp. 1554–1564, Mar. 2018.
- [51] X. Xu, Y. Liu, H. Li, and F. E. Alsaadi, "Robust set stabilization of Boolean control networks with impulsive effects," *Nonlinear Anal., Model. Control*, vol. 23, no. 4, pp. 553–567, Aug. 2018.
- [52] H. Li, X. Xu, and X. Ding, "Finite-time stability analysis of stochastic switched Boolean networks with impulsive effect," *Appl. Math. Comput.*, vol. 347, pp. 557–565, Apr. 2019.
- [53] D. Yang, X. Li, and J. Qiu, "Output tracking control of delayed switched systems via state-dependent switching and dynamic output feedback," *Nonlinear Anal., Hybrid Syst.*, vol. 32, pp. 294–305, May 2019.
- [54] D. Yang, X. Li, J. Shen, and Z. Zhou, "State-dependent switching control of delayed switched systems with stable and unstable modes," *Math. Methods Appl. Sci.*, vol. 41, no. 16, pp. 6968–6983, Aug. 2018.
- [55] J. Fan and L. Li, "Existence of positive solutions for P-Laplacian dynamic equations with derivative on time scales," *J. Appl. Math.*, vol. 2013, no. 3, pp. 1122–1203, 2013.
- [56] A. Luo, "A theory for non-smooth dynamical systems on connectable domains," *Commun. Nonlinear Sci. Numer. Simul.*, vol. 10, no. 1, pp. 21–55, Feb. 2005.
- [57] A. C. J. Luo, "Imaginary, sink and source flows in the vicinity of the separatrix of non-smooth dynamic systems," *J. Sound Vib.*, vol. 285, nos. 1–2, pp. 443–456, Jul. 2005.
- [58] A. C. J. Luo, "The mapping dynamics of periodic motions for a three-piecewise linear system under a periodic excitation," *J. Sound Vib.*, vol. 283, nos. 3–5, pp. 723–748, May 2005.
- [59] A. C. J. Luo and L. Chen, "Periodic motions and grazing in a harmonically forced, piecewise, linear oscillator with impacts," *Chaos, Solitons Fractals*, vol. 24, no. 2, pp. 567–578, Apr. 2005.
- [60] A. Luo and S. Thapa, "On nonlinear dynamics of simplified brake dynamical systems," in *Proc. Int. Mech. Eng. Congr. Expo.*, Washington, DC, USA, 2007, pp. 1849–1859.
- [61] A. Luo, "A theory for flow switchability in discontinuous dynamical systems," *Nonlinear Anal., Hybrid Syst.*, vol. 2, no. 4, pp. 1030–1061, Nov. 2008.
- [62] A. Luo, *Discontinuous Dynamical Systems on Time-Varying Domains*. Beijing, China: Higher Education Press, 2009.
- [63] A. Luo, *Discontinuous Dynamical Systems*. Beijing, China: Springer, 2012.
- [64] D. O'Connor and A. C. J. Luo, "On discontinuous dynamics of a freight train suspension system," *Int. J. Bifurcation Chaos*, vol. 24, no. 12, Dec. 2014, Art. no. 1450163.
- [65] J. Fan, P. Liu, T. Liu, S. Xue, and Z. Yang, "Analysis of discontinuous dynamical behaviors of a friction-induced oscillator with an elliptic control law," *Math. Problems Eng.*, vol. 2018, pp. 1–33, May 2018.
- [66] G. Sun and X. Fu, "Discontinuous dynamics of a class of oscillators with strongly nonlinear asymmetric damping under a periodic excitation," *Commun. Nonlinear Sci. Numer. Simul.*, vol. 61, pp. 230–247, Aug. 2018.
- [67] X. Fu and Y. Zhang, "Stick motions and grazing flows in an inclined impact oscillator," *Chaos, Solitons Fractals*, vol. 76, pp. 218–230, Jul. 2015.
- [68] S. Xue and J. Fan, "Discontinuous dynamical behaviors in a vibro-impact system with multiple constraints," *Int. J. Non-Linear Mech.*, vol. 98, pp. 75–101, Jan. 2018.
- [69] A. C. J. Luo and S. Xing, "Bifurcation trees of period-3 motions to chaos in a time-delayed duffing oscillator," *Nonlinear Dyn.*, vol. 88, no. 4, pp. 2831–2862, Feb. 2017.
- [70] S. Xing and A. C. J. Luo, "On possible infinite bifurcation trees of period-3 motions to chaos in a time-delayed, twin-well duffing oscillator," *Int. J. Dyn. Control*, vol. 6, no. 4, pp. 1429–1464, Mar. 2018.
- [71] A. C. J. Luo and S. Guo, "Period-1 evolutions to chaos in a periodically forced brusselator," *Int. J. Bifurcation Chaos*, vol. 28, no. 14, Dec. 2018, Art. no. 1830046.
- [72] L. Li and A. C. J. Luo, "On periodic solutions of a second-order, time-delayed, discontinuous dynamical system," *Chaos, Solitons Fractals*, vol. 114, pp. 216–229, Sep. 2018.
- [73] S. Chen, J. Fan, and T. Liu, "On discontinuous dynamics of a 2-DOF friction-influenced oscillator with multiple elastic constraints," *Int. J. Non-Linear Mech.*, vol. 110, pp. 131–150, Apr. 2019.
- [74] C. Li, J. Fan, Z. Yang, and S. Xue, "On discontinuous dynamical behaviors of a 2-DOF impact oscillator with friction and a periodically forced excitation," *Mechanism Mach. Theory*, vol. 135, pp. 81–108, May 2019.
- [75] M. Gao and J. Fan, "Analysis of dynamical behaviors of a 2-DOF friction oscillator with elastic impacts and negative feedbacks," *Nonlinear Dyn.*, vol. 102, no. 1, pp. 45–78, Sep. 2020.



JINJUN FAN received the master's degree from Shandong Normal University, in 1988. He is currently a Professor with the Mathematical Department, School of Mathematics and Statistics, Shandong Normal University. His research interests include the discontinuous dynamical systems and nonlinear differential equations.



MIN GAO is currently pursuing the master's degree with the School of Mathematics and Statistics, Shandong Normal University, China. Her current research interest includes the analysis of discontinuous dynamical systems.



SHOULIAN CHEN received the master's degree in mathematics from Shandong Normal University, China. Her current research interest includes the analysis of nonlinear dynamical systems.

...